

AD-A131 851

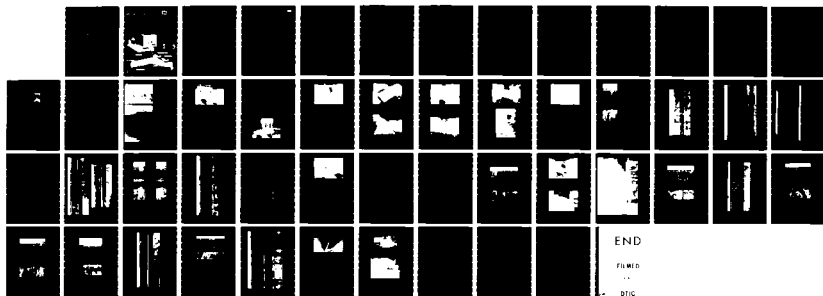
DETECTION OF CAVITIES UNDER CONCRETE PAVEMENT(U) COLD  
REGIONS RESEARCH AND ENGINEERING LAB HANOVER NH  
A KOVACS ET AL. JUL 83 CRREL-83-18 MIPR-CES-82-3

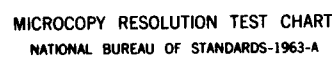
1/1

UNCLASSIFIED

F/G 17/9

NL





MICROCOPY RESOLUTION TEST CHART  
NATIONAL BUREAU OF STANDARDS-1963-A

# CRREL

## REPORT 83-18

ADA 131851

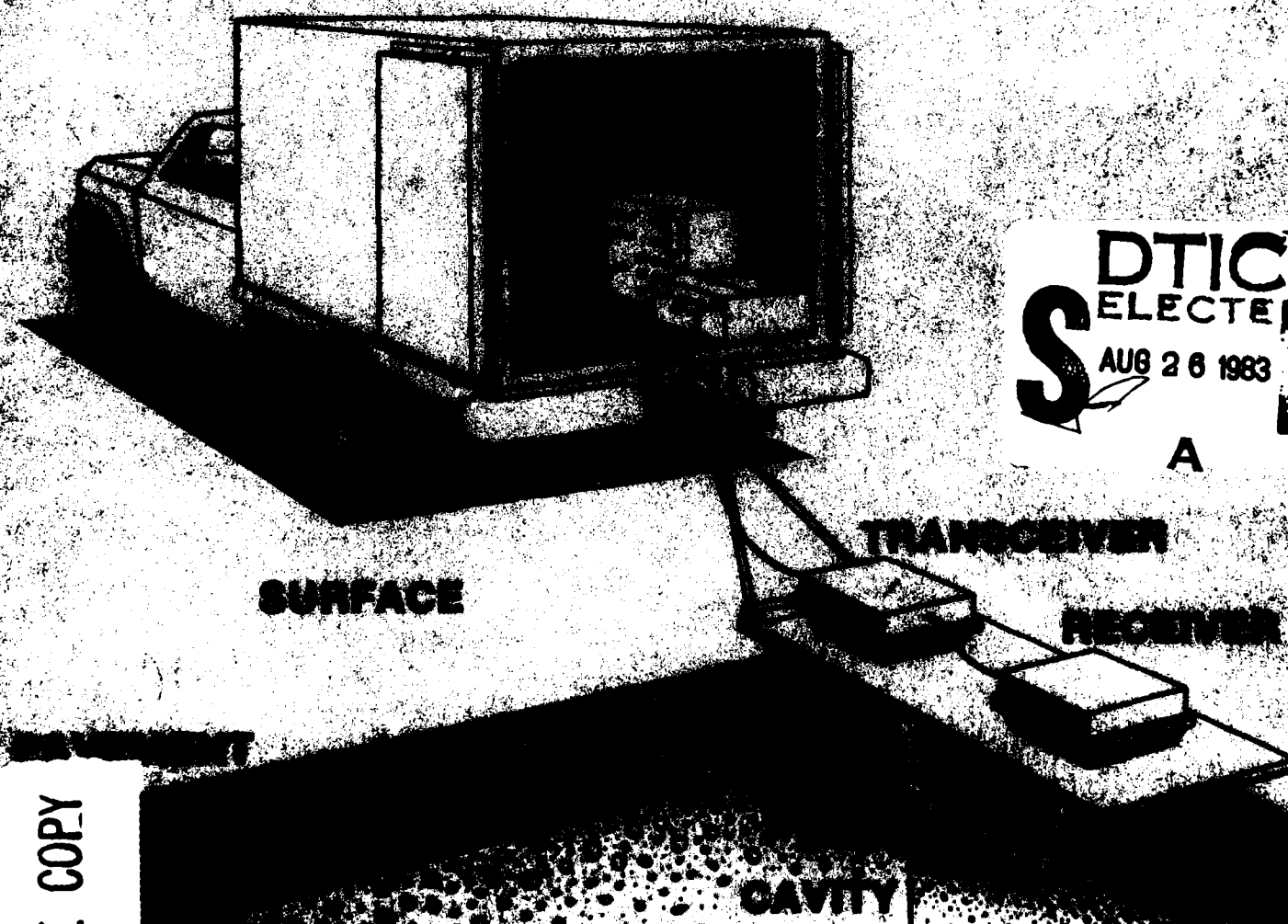


US Army Corps  
of Engineers

Cold Regions Research &  
Engineering Laboratory

(12)

### *Detection of cavities under concrete pavement*



DTIC FILE COPY

This document has been approved  
for public release and sale; its  
distribution is unlimited.

83 08 26 054

*Cover: Arrangement of the impulse radar  
system used for detecting cavities  
under concrete pavement*

# CRREL Report 83-18

July 1983



## *Detection of cavities under concrete pavement*

Austin Kovacs and Rexford M. Morey

Accession For	
NTIS GRA&I	<input checked="checked" type="checkbox"/>
DTIC TAB	<input type="checkbox"/>
Unannounced	<input type="checkbox"/>
Justification	
By	
Distribution/	
Availability Codes	
Dist	Avail and/or Special
A	



Unclassified

SECURITY CLASSIFICATION OF THIS PAGE (When Data Entered)

REPORT DOCUMENTATION PAGE		READ INSTRUCTIONS BEFORE COMPLETING FORM
1. REPORT NUMBER CRREL Report 83-18	2. GOVT ACCESSION NO. AD-A131 851	3. RECIPIENT'S CATALOG NUMBER
4. TITLE (and Subtitle)  DETECTION OF CAVITIES UNDER CONCRETE PAVEMENT		5. TYPE OF REPORT & PERIOD COVERED
		6. PERFORMING ORG. REPORT NUMBER
7. AUTHOR(s)  Austin Kovacs and Rexford M. Morey		8. CONTRACT OR GRANT NUMBER(s)  MIPR CES 82-3 and 82-3A
9. PERFORMING ORGANIZATION NAME AND ADDRESS  U.S. Army Cold Regions Research and Engineering Laboratory Hanover, New Hampshire 03755		10. PROGRAM ELEMENT, PROJECT, TASK AREA & WORK UNIT NUMBERS
11. CONTROLLING OFFICE NAME AND ADDRESS  Office of the Chief of Engineers Washington, D.C. 20314		12. REPORT DATE July 1983
		13. NUMBER OF PAGES 49
14. MONITORING AGENCY NAME & ADDRESS (if different from Controlling Office)		15. SECURITY CLASS. (of this report)  Unclassified
		15a. DECLASSIFICATION/DOWNGRADING SCHEDULE
16. DISTRIBUTION STATEMENT (of this Report)  Approved for public release; distribution unlimited.		
17. DISTRIBUTION STATEMENT (of the abstract entered in Block 20, if different from Report)		
18. SUPPLEMENTARY NOTES		
19. KEY WORDS (Continue on reverse side if necessary and identify by block number)  Cavities Concrete Pavement Radar		
20. ABSTRACT (Continue on reverse side if necessary and identify by block number) An evaluation of an impulse radar system for detecting cavities under concrete pavement is discussed, and field results are presented. It was found that a dual antenna mode of surveying was ideal for void detection. In this mode one antenna operated in a transceive mode and a second, offset from the first, operated in a receive-only mode. This arrangement allowed a refraction-type profile survey to be performed, which enabled subpavement voids to be easily detected. Field trials were held at Plattsburgh Air Force Base, where 28 cavities were detected and mapped. Drilling of holes verified that a cavity existed and allowed cavity depth to be measured. The cavities varied from 1.5 in. to 23 in. in depth and were up to 20 ft long.		

## **PREFACE**

This report was prepared by Austin Kovacs, Research Civil Engineer of the Applied Research Branch, Experimental Engineering Division, U.S. Army Cold Regions Research and Engineering Laboratory, and Rexford M. Morey, Geophysical Systems Consultant, Nashua, N.H. Funding for this study was provided by the Plattsburgh Air Force Base under MIPR No. CES 82-3 and 82-3A.

The authors acknowledge the assistance of Alan R. Greator of CRREL during the field work and Donald Keller, who operated the falling-weight deflectometer and reduced much of the related data. The outstanding support provided by Major Kevin A. Kolz and Roger A. Smart of the Plattsburgh AFB Civil Engineering group, and the many enlisted personnel, who helped in various aspects of the field work, contributed to the speedy completion and success of the field program. Dr. Gordon F.N. Cox provided useful technical counsel. Review of this report was provided by Dr. Ronald Liston and Major Kolz.

## CONTENTS

	Page
Abstract .....	i
Preface .....	ii
Introduction .....	1
Plattsburgh Air Force Base .....	3
Radar sounding system .....	3
Survey procedure .....	9
Cavity inspection .....	10
Radar cavity detection test .....	14
Radar profile results .....	15
Falling-weight deflectometer tests .....	38
Discussion and conclusions .....	41
Literature cited .....	41

## ILLUSTRATIONS

Figure		
1.	Map of the Plattsburgh AFB flight line and runway .....	2
2.	Example of the main aircraft parking apron slab and utility layout .....	4
3.	Example of radar impulse signal vs time and its equivalent real-time graphic display .....	5
4.	Idealization of the development of the graphic record of a pipe signature using impulse radar sounding .....	6
5.	Examples of conical signatures developed by buried objects .....	7
6.	Radar profiling on the Plattsburgh AFB apron .....	8
7.	Schematic of a transceiver antenna impulse ray path to and from a subsurface interface .....	8
8.	Schematic of a refracted ray path .....	8
9.	Coring through the parking apron slab .....	9
10.	Drilling through the parking apron slab .....	10
11.	Inspection hole over the cavity discovered by base maintenance personnel .....	11
12.	View looking southward under slab 38-14L .....	11
13.	Augering a 16-in.-diameter hole into subgrade material .....	12
14.	View of cavity area under key joint between slabs 37-14L and 38-14L .....	12
15.	View of cavity area looking westward under slab 38-14L .....	13
16.	Open key joint between pavement slabs .....	13
17.	Flooding the pavement upslope of the inspection cavity .....	14
18.	Graphic record of radar profile across cavity under slab 38 of rows 14K to 15A .....	15
19.	Example of dual antenna radar profile along row 11A .....	16
20.	Portion of radar profile along row 18K from slab 33 to slab 1 over a 30-in. drain line .....	17
21.	Portion of radar profile along row OM/N from slab 39 to slab 3 over a 30-in. drain line .....	18
22.	Portion of radar profile on row 3B from slab 5 to slab 44 over a 30-in. drain line .....	18
23.	Portion of radar profile on row 5G between slab 44 and slab -1 over a 30-in. drain line .....	20

Figure		Page
24.	Portion of radar profile on row 7J between slab -3 and slab 34 over a 30-in. drain line .....	20
25.	Radar scan across cavity under slab 21 of row 5G .....	21
26.	Radar scan across cavity under slab 6 of row 7J .....	21
27.	Radar profile on row 17A between slab 1 and slab 44 .....	22
28.	Location of cavities under rows 14L and 14M and 17A .....	23
29.	Configuration of cavity under slab 7 of row 17A determined by radar profiling .	24
30.	General locations of cavities found under the flight line and runway pavement at Plattsburgh AFB .....	26
31.	Portion of radar profile on row 4A between slabs 30 and 44 .....	27
32.	Layout of utility fixtures on slab 33 of row 4A and the pavement core taken to allow inspection of the concrete and the subgrade material .....	28
33.	Row 4A, slab 33 pavement core .....	28
34.	Radar profile records showing slab joint features, metal targets and other sub-surface reflection signatures that can be misinterpreted as cavities under concrete pavement .....	29
35.	Radar profile record on apron taxiway .....	37
36.	Corner slab failure .....	38
37.	CRREL trailer-mounted falling-weight deflectometer .....	39
38.	Deflection of four supported slabs and one partially unsupported slab vs distance from the center of the FWD impact plate .....	40

#### TABLE

1.	Location and sizes of subpavement voids .....	25
----	---	----

### CONVERSION FACTORS: U.S. CUSTOMARY TO METRIC (SI) UNITS OF MEASUREMENT

These conversion factors include all the significant digits given in the conversion tables in the ASTM *Metric Practice Guide* (E 380), which has been approved for use by the Department of Defense. Converted values should be rounded to have the same precision as the original (see E 380).

<i>Multiply</i>	<i>By</i>	<i>To obtain</i>
inches	0.254*	metres
feet	0.3048*	metres
pounds	0.4535924	kilograms
pound-force/inches <sup>2</sup> (psi)	6894.757	pascals
yards <sup>3</sup>	0.7645549	metres <sup>3</sup>

\* Exact.

# DETECTION OF CAVITIES UNDER CONCRETE PAVEMENT

Austin Kovacs and Rexford M. Morey

## INTRODUCTION

Surface spalling and D-cracking\* at the corners of the concrete pavement slabs at Plattsburgh Air Force Base, Plattsburgh, New York, is not a widespread problem. However, the corner areas of about a dozen concrete slabs require repair of deteriorated concrete each year. This entails removal of the deteriorated concrete to a depth of 3-4 in., and this cavity is filled with new concrete. Because of the strength and thickness of the over-25-year-old concrete, it was difficult to remove with hand-held equipment. As a result, a large, compressed-air breaker ram (and more recently a hydraulic pavement ram) mounted on a front-end loader is now used. These rams impart high impact loads to the work area.

During routine maintenance in the summer of 1982 the corner of a parking apron slab suddenly cracked through and was driven downward under the blows from the pavement breaker ram. A large cavity could be seen through the resulting hole. The cavity size was made quite apparent when the area around the initial hole was enlarged to about 18 in. wide by 2 ft long. The cavity was up to 8 in. deep and about 8 ft in diameter. It also extended outward from the central area in at least two directions for an unknown distance. The size of this cavity raised considerable concern as to the existence of other subslab cavities and the safety of aircraft using the airfield.

\*D-cracking is fine cracking parallel to concrete joints and along larger slab cracks. D-cracks continue around corners and may progress inward to the center of a slab. A slight darkening or discoloration of the concrete may be the first sign of D-cracking.

Major Kevin A. Kolz of the Civil Engineering Squadron at Plattsburgh AFB brought the discovery of this cavity to the attention of CRREL and asked if the laboratory could provide expertise for determining the origin of the cavity; he also asked if a method existed which could be used to detect other subpavement cavities that may exist under the airfield pavement.

A team from CRREL visited Plattsburgh AFB to inspect the cavity. A preliminary subsurface radar profiling survey was made, using a single radar transceiver antenna, for the purpose of detecting additional voids. In addition, thermal infrared (IR) scanning of the pavement surface was performed to detect subpavement voids. The team provided an initial assessment of the lateral extent of the cavity and suggested that water movement through the pavement joints had caused a reorganization and settlement of the sands which underlie the slabs (Sellmann 1982). The thermal IR measurements revealed many pavement surface anomalies, which may reflect a thermal contrast between slab areas supported and unsupported by the underlying sands (Greatorix 1982). The radar surface profiles were interpreted to indicate "that voids are detected beneath joints in all runs" and "in at least one case there are obvious voids located beneath the concrete" slabs (Dean 1982). This survey was made over a very limited area of the parking apron; apparently fewer than 20 slabs were profiled.

While no drill holes were made to verify these speculative IR and radar findings, the possibility that the airfield pavement may be undermined with voids created further concern. As a result, a more detailed study was undertaken by the authors. Subsurface radar sounding was again used, along with direct

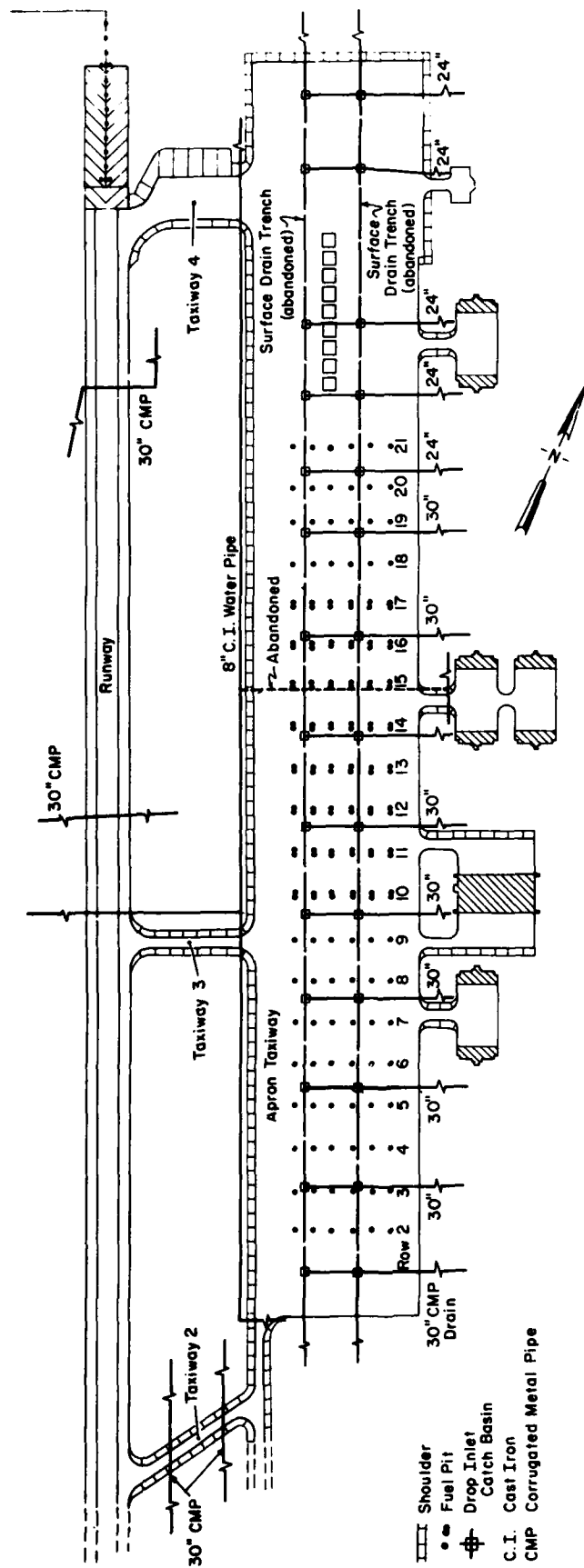


Figure 1. Map of the Plattsburch AFB flight line and runway showing numbered fuel pit rows and water and drainage utility systems under the airfield pavement. The hatched areas are hangars.

measurement provided by core and drill holes through the slabs. A falling-weight deflectometer (FWD) was also used to evaluate the responses of unsupported vs fully supported slabs.

The objectives of this study were 1) to determine if the remote-sensing IR and radar systems had indeed detected the presence of subslab voids, 2) to evaluate if the radar system can be configured for detecting subslab voids, 3) to locate other cavities which may exist under the airfield pavement, 4) to explore the potential use of the FWD as a nondestructive device to verify the existence of subslab voids, and 5) to determine what phenomenon is responsible for the formation of the cavities.

### PLATTSBURGH AIR FORCE BASE

The Plattsburgh AFB was constructed in the mid-1950s. The parking apron and runway complex (Fig. 1) were constructed of nonreinforced concrete 12-14 in. thick (actual field measurements). Joints that run in a south-southeast to north-northwest direction, or along the major axis of the apron and runway, are keyed joints spaced 20 ft apart. Joints perpendicular to these key joints are dummy joints cut 2-3 in. into the concrete. The dummy joints are typically 20 ft apart, but there are rows where these joints are closer together or up to 10 ft farther apart. All joints were originally filled with a compliant sealer.

The parking apron is about 1150 ft wide from shoulder to shoulder. At the southern end the concrete surface has a patchy brown discoloration. This staining is believed to be caused by dissolved iron in water which has been seen to move upward through the pavement joints when the water table is high. The existence of this staining suggests that the subgrade under this area of the parking apron consists of iron-rich sands.

The surface of the parking apron slopes from the west to the east. As a result, runoff flows diagonally across the apron from the runway side to the support facility side of the apron (Fig. 1). Taxiways leading from the apron slope downward to the runway, which is several tens of feet lower than the west side of the parking apron.

Underlying the airfield pavement are a number of electrical, water, fuel and drainage systems. The water and drainage systems are shown in Figure 1. A representative area of the parking apron from fuel pit row 14 to just beyond fuel pit row 17 is shown in Figure 2. This figure shows the relative dimensions

of the pavement slabs and fuel pits (a-f) and the location of service lines, an electric and water main, an active drainage line, and the abandoned surface drainage trenches. Other features of the parking apron pavement include steel-bar tiedown points and steel utility covers.

### RADAR SOUNDING SYSTEM

The radar sounding system operates as an echo sounding device, and has been previously described by Morey (1974). The system includes timing electronics, which clock an impulse generator and sampling head. The impulse source generates a 60- to 100-V electromagnetic (EM) wavelet. The wavelet radiated from the linearly polarized bow-tie-shaped antenna we used had a spectrum of approximately 550 MHz, with 3-dB points of the spectrum at about 400 and 700 MHz. The radiated time-domain wavelet was about 5 ns long. One antenna element was used for transmission and one as a receiver. They were set back from each other so that their long axes were parallel. The center spacing between the elements was about 6 in. These were enclosed in a 1-ft-wide by 1.2-ft-long by 5-in.-high housing. This dual-element transceiver system will be referred to as one antenna.

The transmitted EM wavelet that is not scattered or absorbed is reflected back to the antenna from various interfaces or anomalies within the medium being sounded. The received signal is then displayed on a graphic recorder, similar to the way information is recorded from an acoustic subseabottom profiling system. An example of a received or reflected wavelet is illustrated in Figure 3. The graphic record is a display of the travel time of the wave to various reflecting interfaces and back to the antenna, or the two-way travel time of the wavelet. The depth of penetration and the propagation velocity of the radiated EM wave in the medium being sounded are functions of water content, mineral composition, temperature, grain size, pressure, porosity, conductivity, etc. as well as system performance characteristics. A further discussion of EM energy dissipation processes is beyond the scope of this text. Suffice it to say that the sounding depth or range of the radar system varies from a few inches to many tens of feet as affected by the attenuation and scattering characteristics of the medium being probed.

To convert the two-way travel time (as displayed on the graphic record) to depth, one must know the effective propagation velocity of the EM wavelet

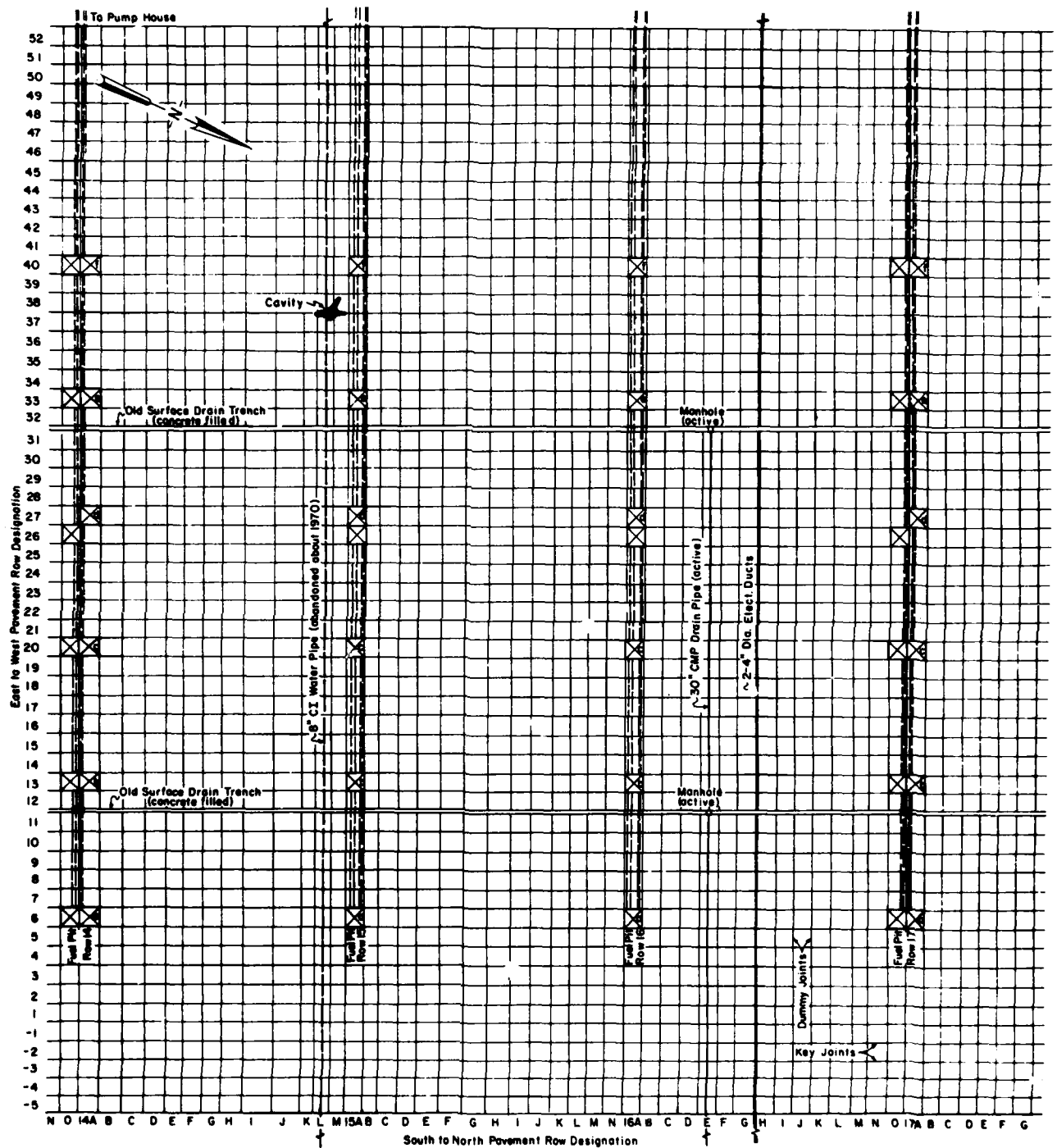


Figure 2. Example of the main aircraft parking apron slab and utility layout.

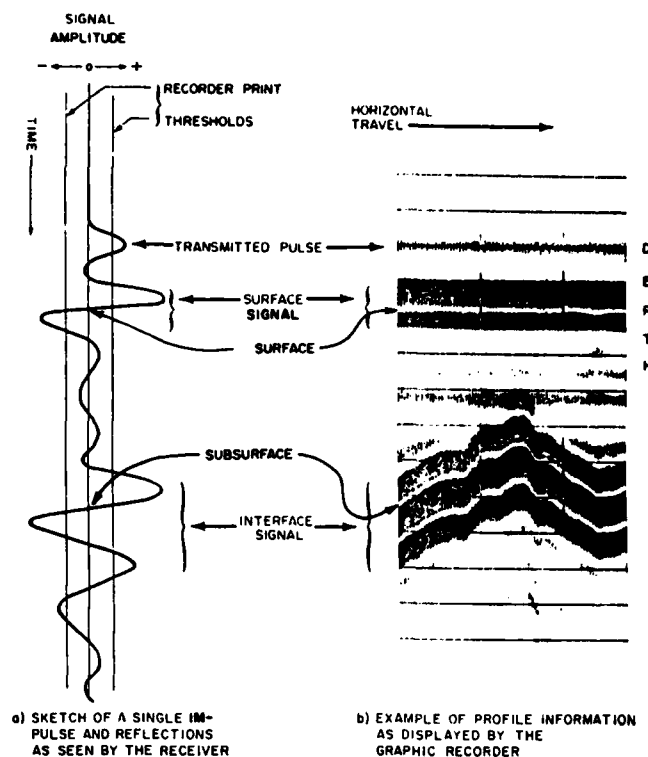


Figure 3. Example of radar impulse signal vs time and its equivalent real-time graphic display. Horizontal scan lines in the graphic record represent equal time intervals, which can be converted to a depth scale.

within the intervening medium. Depth can then be estimated from

$$D = \sqrt{\left(\frac{t_D V}{2}\right)^2 - \frac{S^2}{4}} \quad (1)$$

where  $D$  = depth

$V$  = effective propagation velocity

$t_D$  = travel time to and from the subsurface interface

$S$  = distance between the transmit and receive antenna elements.

The effective propagation velocity of the EM wave in a medium can be calculated from

$$V = \frac{c}{\sqrt{\epsilon'}} \quad (2)$$

where  $c$  = electromagnetic velocity in free space  
 $\approx 11.8$  in./ns

$\epsilon'$  = real effective dielectric constant of the medium.

For homogeneous materials such as water or solid freshwater ice the real effective dielectric constant is known ( $\approx 80$  for water at  $20^\circ\text{C}$ ,  $\approx 3.2$  for solid ice at  $-10^\circ\text{C}$ ). But the real effective dielectric constant of most materials in situ is unknown because this value is affected, to varying degrees, by the parameters previously listed. Therefore, to convert the two-way travel time to an interface to depth, one can use a depth measurement in a pit or drill hole to the interface. Provided subsurface conditions do not change, it is then possible to use the measured depth to the first interface to scale the relative depths to other interfaces. One can also estimate the real effective dielectric constant from published values for the material being sounded. For example, the real effective dielectric constant for concrete varies from about 6 when dry to about 12 when saturated. Likewise, the real effective dielectric constant is about 3 for dry sand in situ and about 30 for sand saturated with water. A representative value of  $\epsilon'$  for well-drained sand in situ is about 4.

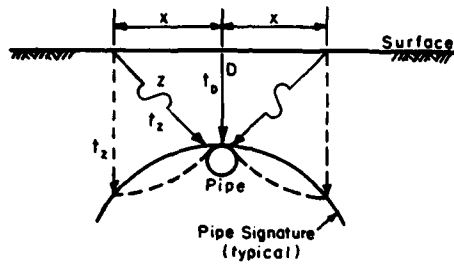


Figure 4. Idealization of the development of the graphic record of a pipe signature using impulse radar sounding.

For a pipe or similar buried target the situation for determining its depth can be as follows. As the antenna approaches and passes over the pipe, the antenna "sees" the pipe at some distance before and after it moves over the buried object. Figure 4 illustrates how a pipe signature is developed. The signature can be used to find the depth to the object when only a distance along the ground and a time ratio are known; the time ratio can easily be scaled off the graphic time record.

As the antenna approaches the target, the object comes into the field of detection. This occurs when the angle between the target and the antenna is approximately  $45^\circ$ . The EM wavelet reflected from the target is displayed on the graphic record as the two-way slant range travel time  $t_z$ . This travel time occurs along a distance  $Z$ , which is greater than the actual depth  $D$  of the target. As the antenna approaches the target, the EM wavelet travel time approaches the shortest time of flight, which occurs when the antenna is directly over the target. Buried objects are therefore detected on the graphic record by the distinctive conical or inverted U-shaped signature, such as that shown in Figure 5. The "tails" on either side of the buried target are therefore the slant-range reflection from the target as the antenna is moved toward or away from the target.

It is assumed that the electrical properties of the subsurface material along path  $Z$  in Figure 4 are, on the average, equal to those along path  $D$ , and that the pipe dimensions are insignificant relative to the other dimensions in the figure. The following relations may then be used to determine the pipe depth:

$$X^2 + D^2 = Z^2 \quad (3)$$

where  $X$  is a distance extending from over the center of the pipe outward along the ground, and

$$\frac{t_D}{t_z} = \frac{D}{Z} \quad (4)$$

where the slant-range travel time  $t_z$  is equal to  $2/V \cdot \sqrt{D^2 + X^2}$ .

By combining eqs 3 and 4 and solving for  $D$  we obtain

$$D = X \sqrt{\frac{1}{\left(\frac{t_z}{t_D}\right)^2} - 1} \quad (5)$$

This equation requires only that the distance along the surface be known and that a time ratio ( $t_z/t_D$ ) with no dimensions be scaled off the graphic record.

For detecting cavities under the pavement at Plattsburgh AFB, the profiling arrangement shown in Figure 6 was used. As shown, two antennas were dragged on a wooden sled behind a truck. One antenna was used as a transceiver while the second was used in the receive-only mode. The EM wave or ray path shown for the transmit-receiver antenna arrangement in Figure 7 is illustrative of reflection profiling, and eq 1 may be used to estimate the depth to an interface. Our radar antennas were 42 in. apart. The resulting idealized refraction EM ray path is depicted in Figure 8. In this case the expression for time  $t$  for the EM ray path shown is

$$t = 2D \left[ \frac{V_2^2 - V_1^2}{V_1 V_2} + \frac{S}{V_2} \right] \quad (6)$$

where  $V_1$  and  $V_2$  = effective propagation velocity in media 1 and 2, respectively  
 $S$  = antenna separation distance.

This equation holds when the angle of incidence  $I$  of the electromagnetic wave at the interface is such that the refracted angle  $R_f$  is  $90^\circ$  and  $V_2 > V_1$ , or  $\epsilon'_1 > \epsilon'_2$  and  $S > 2V_1 D / (V_2^2 - V_1^2)^{1/2}$ . Here  $\epsilon'_1$  and  $\epsilon'_2$  are the real effective dielectric constants of media 1 and 2, respectively. The angle of incidence  $I$  of the EM wave impinging on the interface is, from Snell's law,  $\sin^{-1}(V_1/V_2)$ . Since

$$V_1/V_2 = (c/\sqrt{\epsilon'_1})/(c/\sqrt{\epsilon'_2}) = \sqrt{\epsilon'_2/\epsilon'_1} \quad (7)$$

it then follows that

$$I = \sin^{-1} \sqrt{\epsilon'_2/\epsilon'_1} \quad (8)$$

In this study we assumed that for the moist concrete pavement  $\epsilon'_1$  was 7.5 and for the underlying sand  $\epsilon'_2$  was 4.5. It follows, then, that  $I = \sin^{-1} \sqrt{4.5/7.5} \approx 51^\circ$ . Likewise, where a cavity exists under the slab and  $\epsilon'_2$  for air = 1, then  $I$  is  $\sin^{-1} \sqrt{1/7.5} \approx 21^\circ$ . The effective propagation velocity of the EM wave is determined from eq 2 to be 4.3 in./ns in the concrete, 5.6 in./ns in the sand, and 11.8 in./ns in the air in a cavity.



*a. Buried telephone cable and pipe. The horizontal scale lines are 40 ns apart.*

*b. Buried crevasse in firn on the Ross Ice Shelf, Antarctica. The scale lines are 100 ns apart.*

*Figure 5. Examples of conical signatures developed by buried objects. The width of the conical signature is a function of antenna ground speed, depth and size of target, and subsurface conditions.*

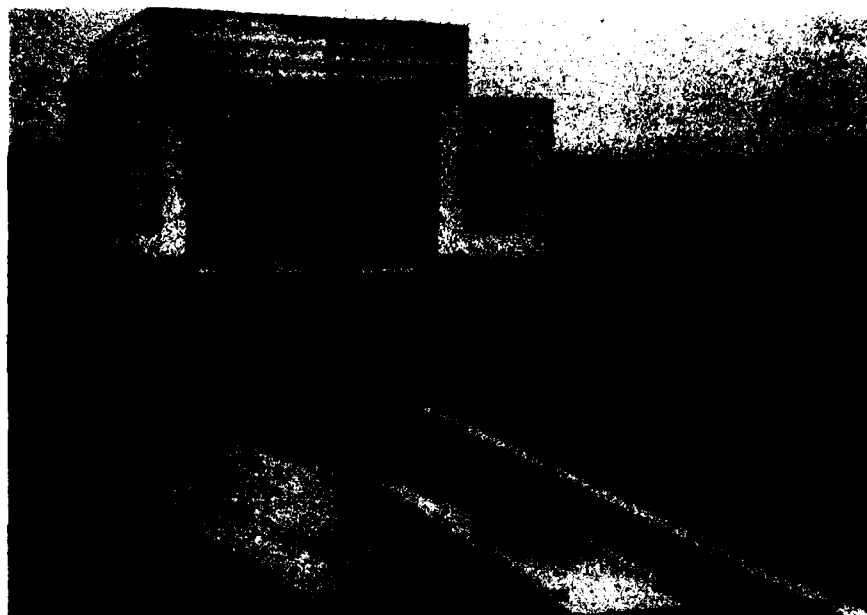


Figure 6. Radar profiling on the Plattsburgh AFB apron. The radar console is at the operator's left. Two antennas are on the wooden sled.

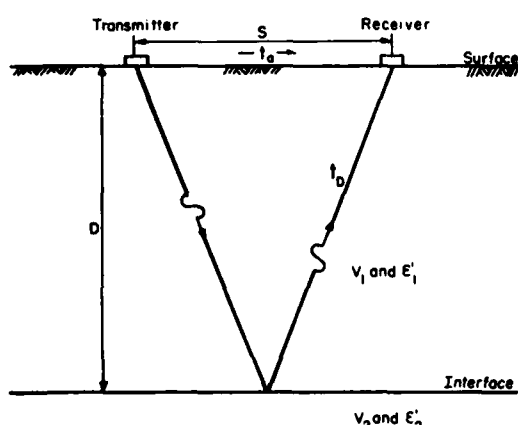


Figure 7. Schematic of a transceiver antenna impulse ray path to and from a subsurface interface. Here  $t_a$  is the air-wave travel time from the transmitter to the receiver element.

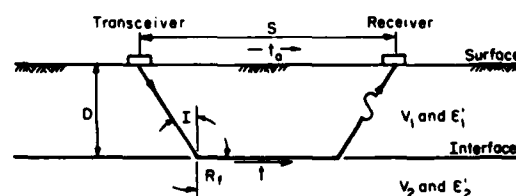


Figure 8. Schematic of a refracted ray path.

Using these velocity values and an antenna separation distance of 42 in. in eq 6, we calculated that the flight time  $t$  for the EM wavelet along the ray path depicted in Figure 8 is 11.7 ns when the concrete is in contact with sand and 9.6 ns when it is in contact with air. The effect of a cavity under the pavement, then, is to decrease the EM-wave travel time from the transceiver to the receive-only antenna by about 2 ns. This time difference should produce a positive visual hump in the graphic record from the receive-only antenna. In short, the interface at the bottom of the concrete should appear to rise up over a cavity. We looked for this time change on the graphic record to discover cavities under the airport pavement.

### SURVEY PROCEDURE

Radar profiles were run across each parking apron slab beginning at slab 1 on the east side of the apron and moving westward to slab 44 (Fig. 2). Beyond slab 44 was the apron taxiway area, which was surveyed from south to north. The apron east of row 1 consisted of five slab rows which were used for vehicle traffic and storage; these slabs were designated rows -1 through -5 and were only surveyed if a utility line passed under them. Each profile run was made at a slow walk, with the antenna sled typ-

ically pulled parallel to, but 3 ft offset from, a dummy joint. One side of each slab was surveyed. Selected pavement areas were also profiled on the taxiways and the runway. The survey was delayed at times by aircraft operations, and the area available to be profiled was dictated by aircraft parking assignments. However, these delays were reduced to minor inconveniences by the helpful flight-line and maintenance staff. Areas not profiled included the taxiways to the hangers, the apron area in front of the hangars (Fig. 1), and the main apron area north of row 21H and east of the west surface drain trench, which was not made available to us. In addition to the profiling run beside the slab joints, profile runs were made over all buried utility lines and along the abandoned surface drain trench.

Anomalous features that appeared in the radar graphic record but did not produce the unique time hump indicating a cavity were explored by coring a 6-in.-diameter hole through the pavement (Fig. 9). Later in the study smaller-diameter holes were drilled with a jackhammer (Fig. 10) to verify that the radar had found another cavity. Since this was a study to verify a preconceived cavity detection concept, it was imperative that these features be examined to ensure that they were not cavities. In the same fashion, sites where the graphic record indicated a cavity were also drilled, and the cavity depth was measured with a tape.

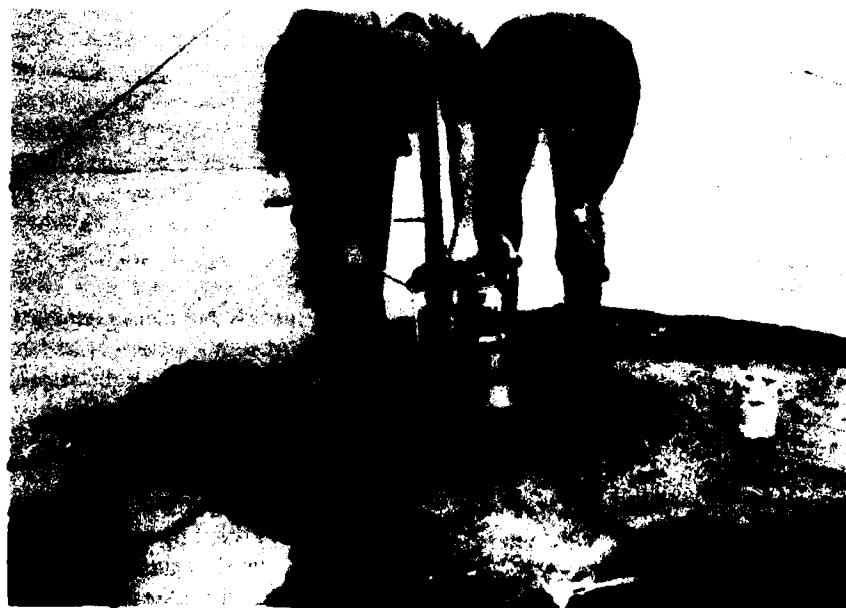


*Figure 9. Coring through the parking apron slab.*



*Figure 10. Drilling through the parking apron slab.*

#### CAVITY INSPECTION

The cavity discovered by the base maintenance personnel was inspected on the first day of our study. The inspection opening cut through the concrete (Fig. 11) was located on slab 38 of Row 14L as shown in Figure 2. A view looking under the slab along the key joint is shown in Figure 12. The severed section of concrete resting on the bottom of the cavity is nearly 15 ft long. This piece of concrete is believed to have been broken off by the concrete breaker when the inspection hole was drilled.

A 16-in.-diameter power auger was used to drill a hole into the subgrade sand to a depth of 4 ft below the bottom of the concrete pavement (Fig. 13). The hole was drilled to determine if coarse gravel existed at depth into which sand may have migrated downward, thus allowing the cavity to form. No gravel was penetrated.

Standing in the augered hole provided a clear view of the cavity area under the pavement. The relative shape of the cavity resembled that shown in Figure 2. The cavity had a maximum depth of about 8 in. and extended southward under the key joint between slabs 37 and 38 to row 14J. This subslab cavity is shown in Figure 14. The face of slab 37 below the key is at position 1. Numerous water stains were along this surface. The concrete broken from the bottom of slab 38 is at position 2. This broken piece extends about 15 ft beyond the camera's view. Position 3 is the bottom of slab 38, and number 4 is

the top of the subgrade sand. The latter area is higher than position 5, which is a trench in the sand directly below the key joint. The surface of this trench slopes upward to the rear of the photo. Note that the bottom of the trench is dark due to higher moisture on the surface.

Another major fork of the cavity extended diagonally across the dummy joint between slabs 38-14L and 38-14M. This area is shown in Figure 15. The bottom of the pavement has a rough-textured surface. The subgrade sand surface has a rolling, subdued topography. This morphology is indicative of the erosion relief produced by flowing water. The source of this water would be from pavement surface drainage through the slab joints. Along many joints the expansion mastic has long deteriorated, leaving cracks and holes through the material. In numerous places the dried-out sealant has been swept or vacuumed out during routine pavement cleaning. Figure 16 shows a key joint with a section of its joint sealer removed and a large hole through the sealer just below the junction of four slabs.

To verify that surface water would rapidly enter the joints and to see how the water would move under the slabs surrounding the cavity, a water truck was used to flood the pavement upslope of the cavity (Fig. 17). While water drained into most of the joints, the majority of the surface flow entered the key joints. These joints were wide and offered good drainage to the base of the slabs. Water first entered the key joint at the arrow in Figure 17. When the



*Figure 11. Inspection hole over the cavity discovered by base maintenance personnel. The arrow points to the 2.5-in. saw-cut dummy joint surface. The key extending from the slab (upper right) is apparent, as is the subgrade sand at the bottom of the cavity.*



*Figure 12. View looking southward under slab 38-14L. Slab 37-14L is at the left arrow. A concrete section broken from slab 38-14L is at the right arrow. The two surfaces were once in contact below the key, which projects out just above the left arrow.*

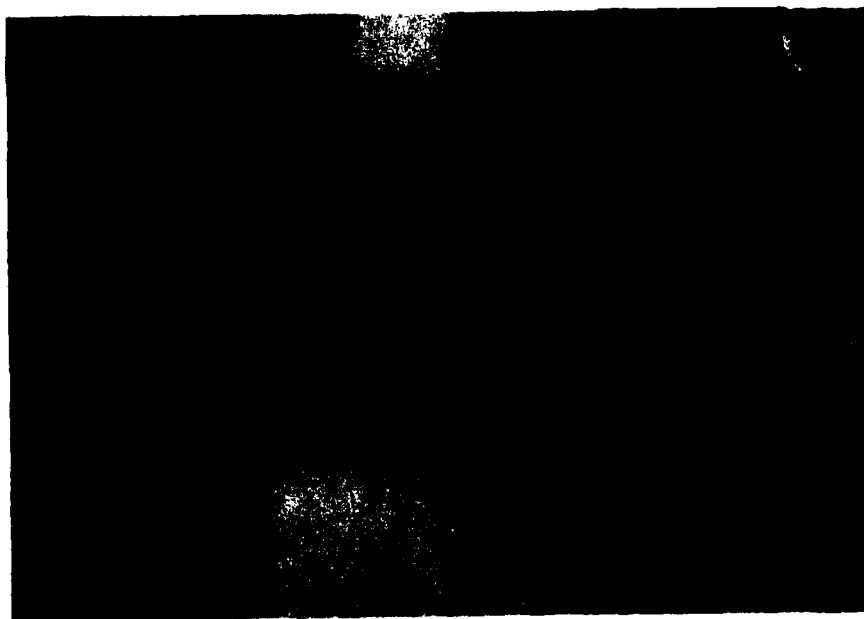


*Figure 13. Augering a 16-in.-diameter hole into subgrade material.*



*Figure 14. View of cavity area under key joint between slabs 37-14L and 38-14L.  
(Photo by A.R. Greatorex.)*

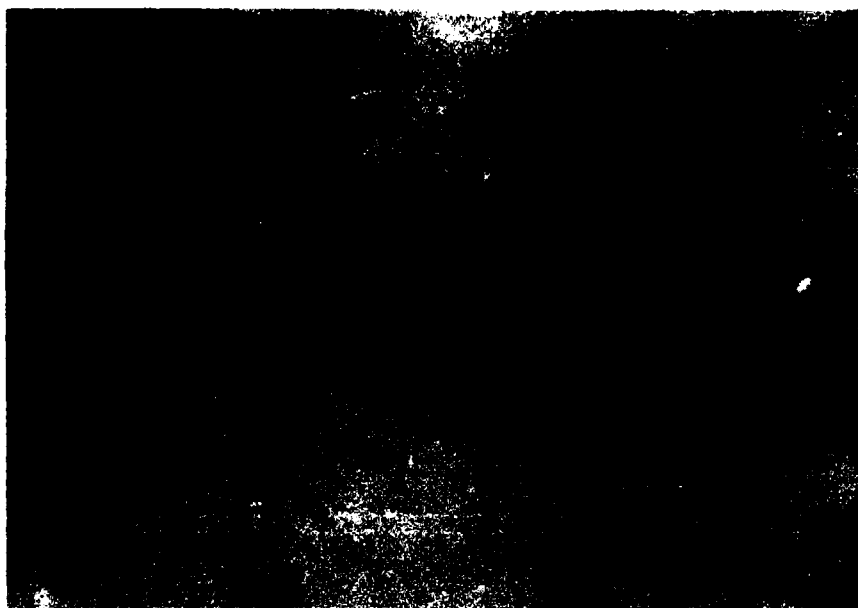


*Figure 15. View of cavity area looking westward under slab 38-14L. (Photo by A.R. Greatorex.)*



*Figure 16. Open key joint between pavement slabs.*

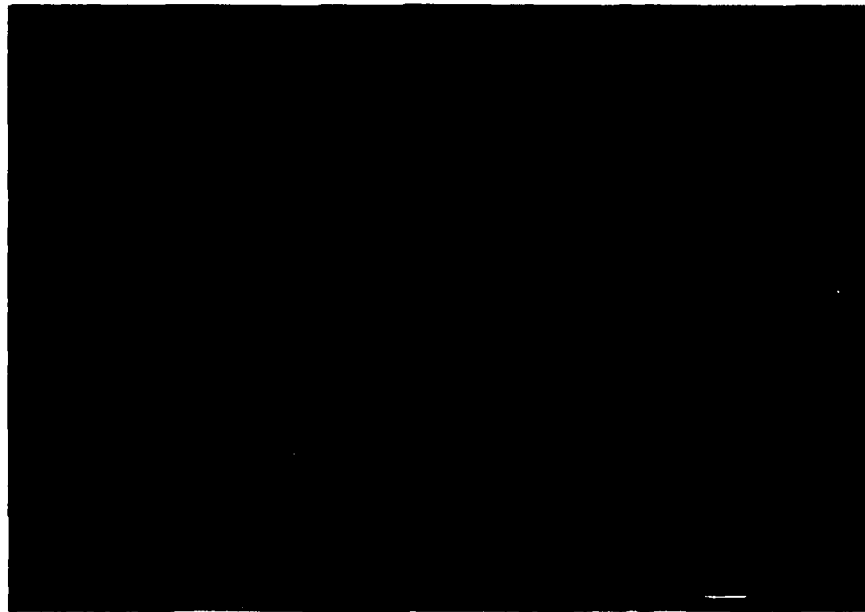


*Figure 17. Flooding the pavement upslope of the inspection cavity, which is surrounded by a sand berm.*

underlying material became "saturated," infiltration slowed and the joint filled with water. Surface water then overflowed the joint and moved farther down the apron slope. Standing in the augered hole and looking out under the pavement, we first observed water moving toward the hole along the diagonal trench extending to the general position of the arrow in Figure 17. When the surface water reached the key joint between slabs 37 and 38, water poured through, rapidly saturated the sand, and then moved quickly toward the augered hole. Within a very short time this hole filled with water, followed by the entire cavity. The water from the tanker was then shut off and the rate of drawdown was measured. This occurred at a uniform rate of 0.5 in./min until all the water had percolated away. Some slumping of the subgrade around the augered hole occurred, as would be expected with water flowing over the lip of a hole in sand. The surface morphology of the outlying cavity also seemed to change but we could not verify this. It was clear, however, that surface water could freely enter the key joints and move rapidly along the cavity floor from all directions to the center of the cavity. This implied that the center of subgrade subsidence was below the area of the opening in the pavement and that the underlying sand was not being transported horizontally away from the area along the trenches.

This finding drew our attention to the 8-in. cast-iron water pipe which runs under the pavement near

the cavity (Fig. 2). Mr. Francis Patnode, who had been associated with various aspects of the Plattsburgh AFB facilities engineering and maintenance since its construction, told us that this pipe was abandoned about ten years ago because it was found to be leaking. On rare occasions, when the water table was high, water from the pipe had actually been seen rising through the pavement joints onto the surface in what he believed to be the area of the existing cavity. From our previous observations and this knowledge, we concluded that the cavity had formed as a result of sand migration into this broken utility line.

#### **RADAR CAVITY DETECTION TEST**

Radar profile test runs were made on slabs in the area of the cavity. The purpose was to verify that the radar could detect a subpavement cavity, to determine what this feature would look like on the graphic record, and to verify that the refracted wavelet flight time would be less under an unsupported than under a supported pavement and that this time foreshortening would produce a positive hump in the graphic record of the receive-only antenna.

A number of test runs were made. The results are shown in Figure 18, which is the graphic record of a profile down the center of pavement slabs 38-14K to 15A. The data from the transceiver antenna are displayed in the upper half of the graphic record (section A)

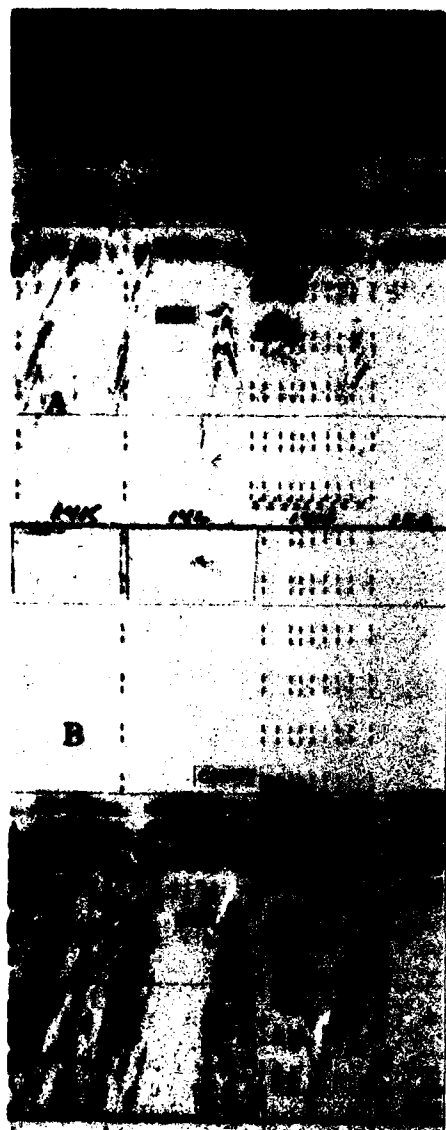


*Figure 18. Graphic record of radar profile across cavity under slab 38 of rows 14K to 15A. The distance between the horizontal scale lines is 10 ns. Note the conical signature developed as the antennas moved across the buried pipe. (The next-to-last 2-ft event mark on the right side of slab 38-14M did not print. Also, two of the 2-ft event marks did not carry down through the bottom half of the record.)*

and the data from the receive-only antenna are in the lower half (section B). The widely spaced vertical event marks represent the location of each dummy joint crossed, while the closely spaced vertical event marks represent scale marks painted at 2-ft intervals on the pavement surface.

In trace A the transmitted EM wavelet is quite evident and allows the relative position of the concrete surface to be determined. The bottom of the concrete, the signature of a buried pipe, and the "bright spot" feature associated with the cavity are shown. The contrast between the wavelet reflected from the concrete/sand interface vs the concrete/air interface is quite evident. The amplitude of the reflected signal is a function of the dielectric contrast at the interface. The EM wavelet energy reflected from a concrete/sand interface vs that from a concrete/air interface may be determined from the reflection coefficient  $\rho = (\sqrt{\epsilon'_1} - \sqrt{\epsilon'_2}) / (\sqrt{\epsilon'_1} + \sqrt{\epsilon'_2})$ . Using an  $\epsilon'_1$  value of 7.5 for moist concrete and  $\epsilon'_2$  values of 1 for air and 4.5 for sand, we calculated the reflection coefficient at a concrete/air interface to be 0.47 and at a concrete/sand interface to be 0.13. The reflected energy from the concrete/air interface is about three times higher than that from a concrete/sand interface. This is why the graphic record is so much darker over the cavity.

The transmitted wavelet,  $t_a$  in Figure 7, which can travel from the transceiver antenna through the air to the receive-only antenna is not displayed in trace B because the antennas are shielded. The flight time of this air wave was not needed in this study, but it is needed in analyzing some dual-antenna survey data (Kovacs et al. 1982). When needed, this air wave can be detected by simply lifting the adjacent sides of each antenna slightly so that the transmitted wavelet can travel from between the antennas without being blocked by the antenna side-wall shielding.

The first return displayed in trace B of Figure 18 is the refracted wavelet from the bottom of the concrete pavement. The important feature in this trace is the shortened time hump over the cavity. This result verified that the proposed methodology using dual-antenna impulse radar sounding was appropriate for detecting cavities under concrete pavement.

## RADAR PROFILE RESULTS

Radar profiles were run across all of the main apron slabs except for the restricted area at the northeast end of the apron. In addition, radar profiles were made along each of the buried utility lines under the runway, taxiways and main parking apron, again except for those in the restricted area.

A representative profile of the parking apron is shown in Figure 19. This profile was run on row 11A beginning at slab 1 and ending at slab 44. Certain features in this profile will appear in many of the following profiles run in the same direction on the apron. For example, the vertical event marks indicate

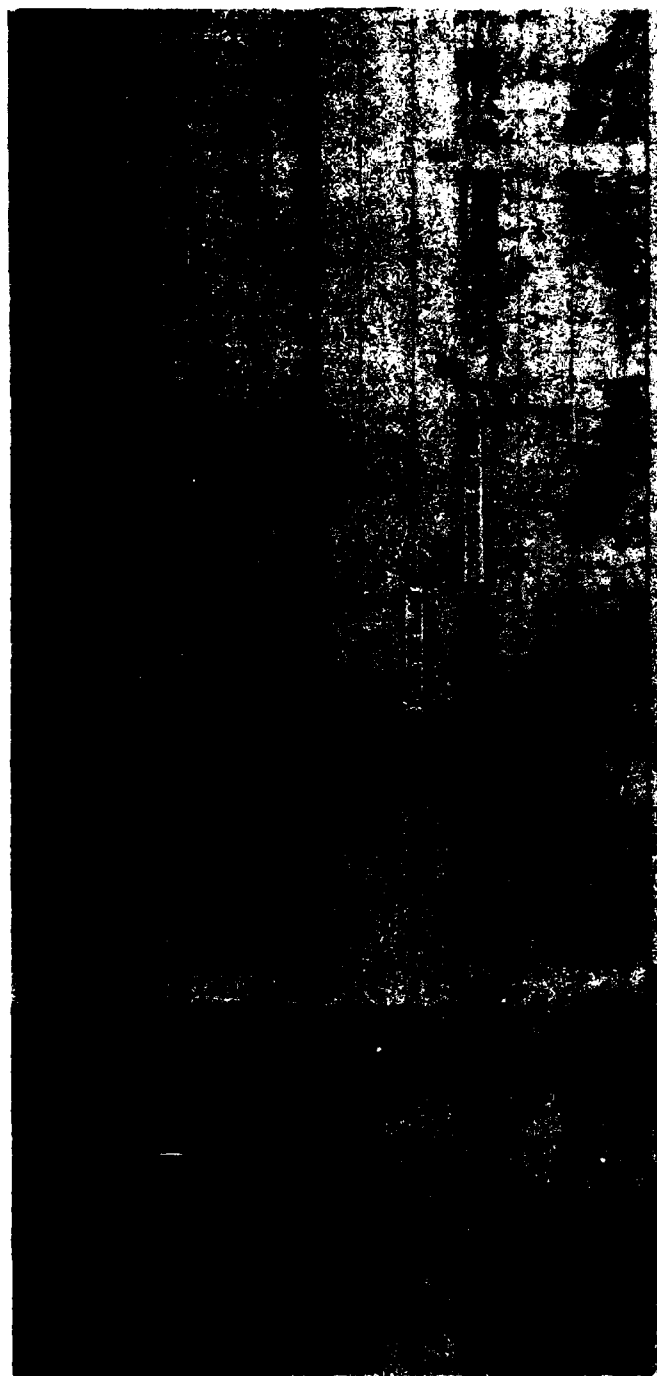


*Figure 19. Example of dual antenna radar profile along row 11A. This profile was run from slab 1 to slab 44 (see slab numbers at bottom of trace A). The horizontal scale lines are 5 ns apart.*

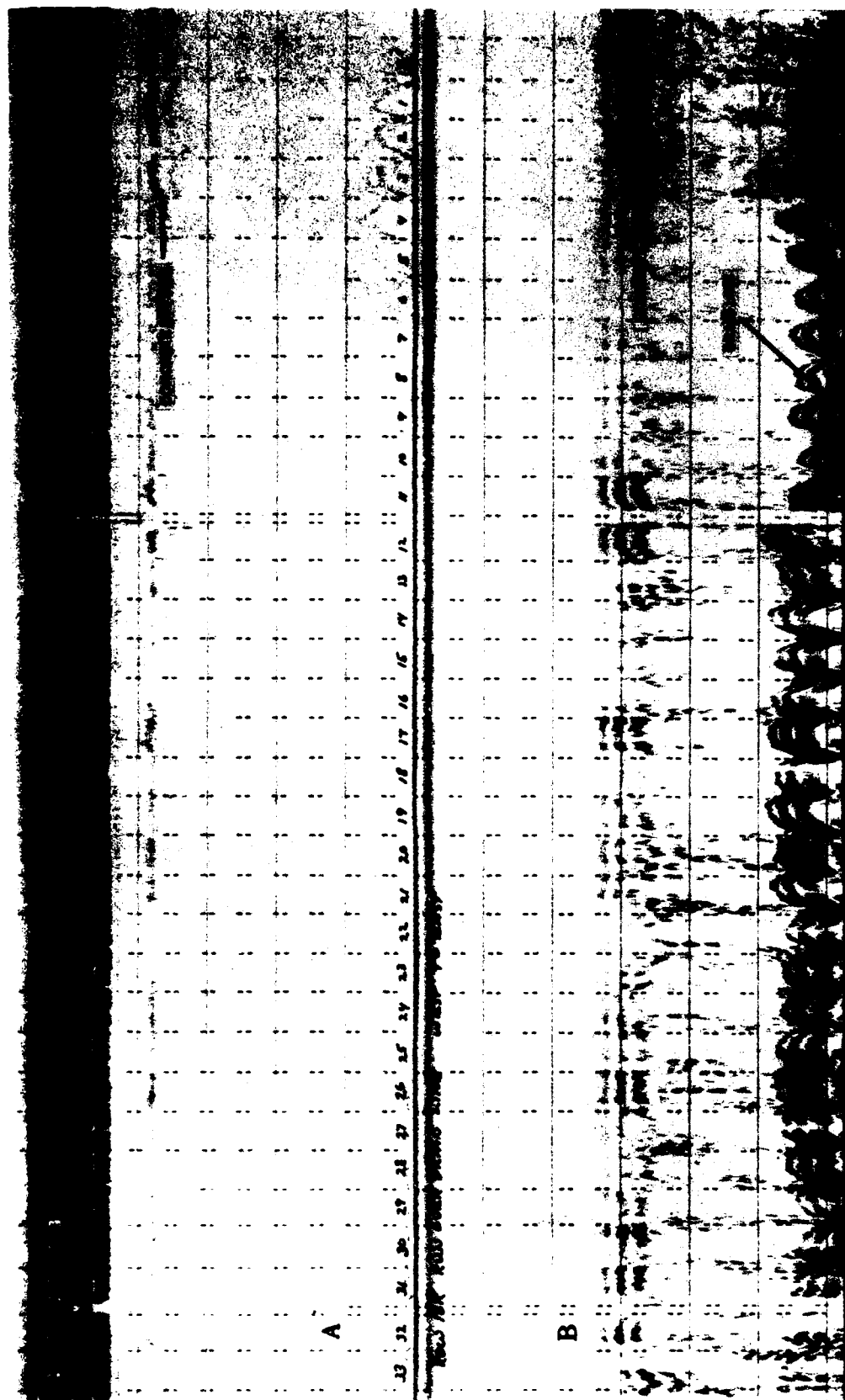


Figure 20. Portion of radar profile along row 18K from slab 33 to slab 1 over a 30-in. drain line. The scale lines are 5 ns apart.

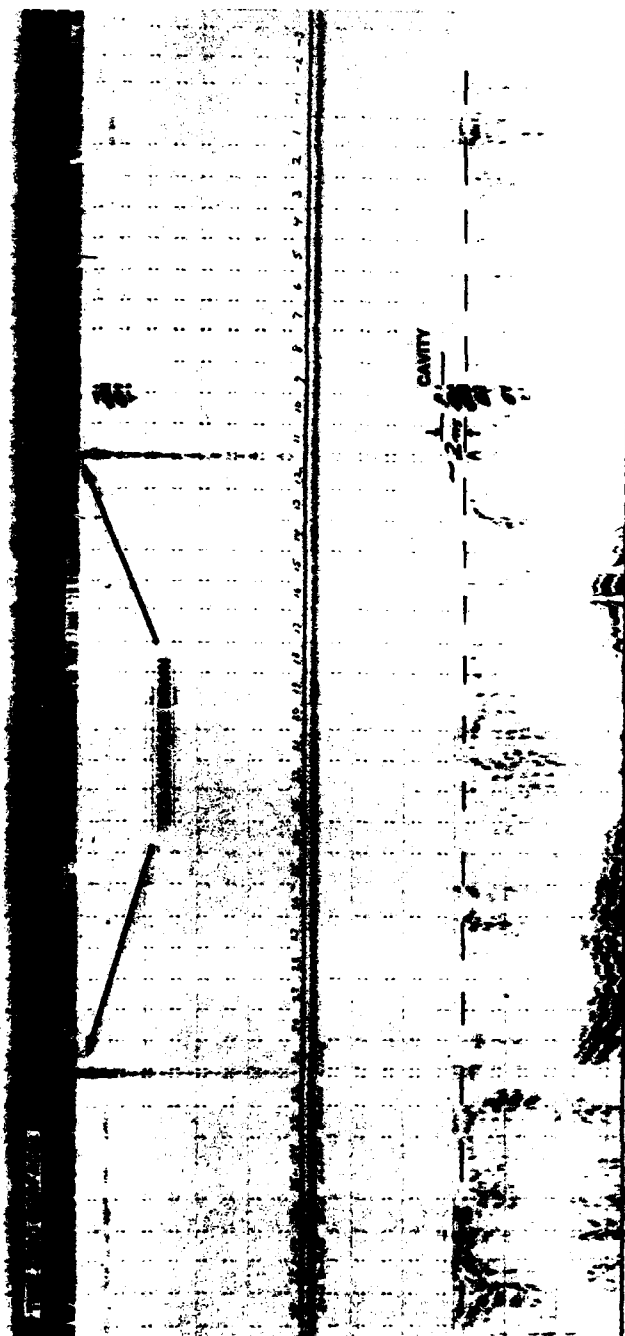


Figure 21. Portion of radar profile along row OM/N from slab 39 to slab 3 over a 30-in. drain line. The scale lines are 5 ns apart.

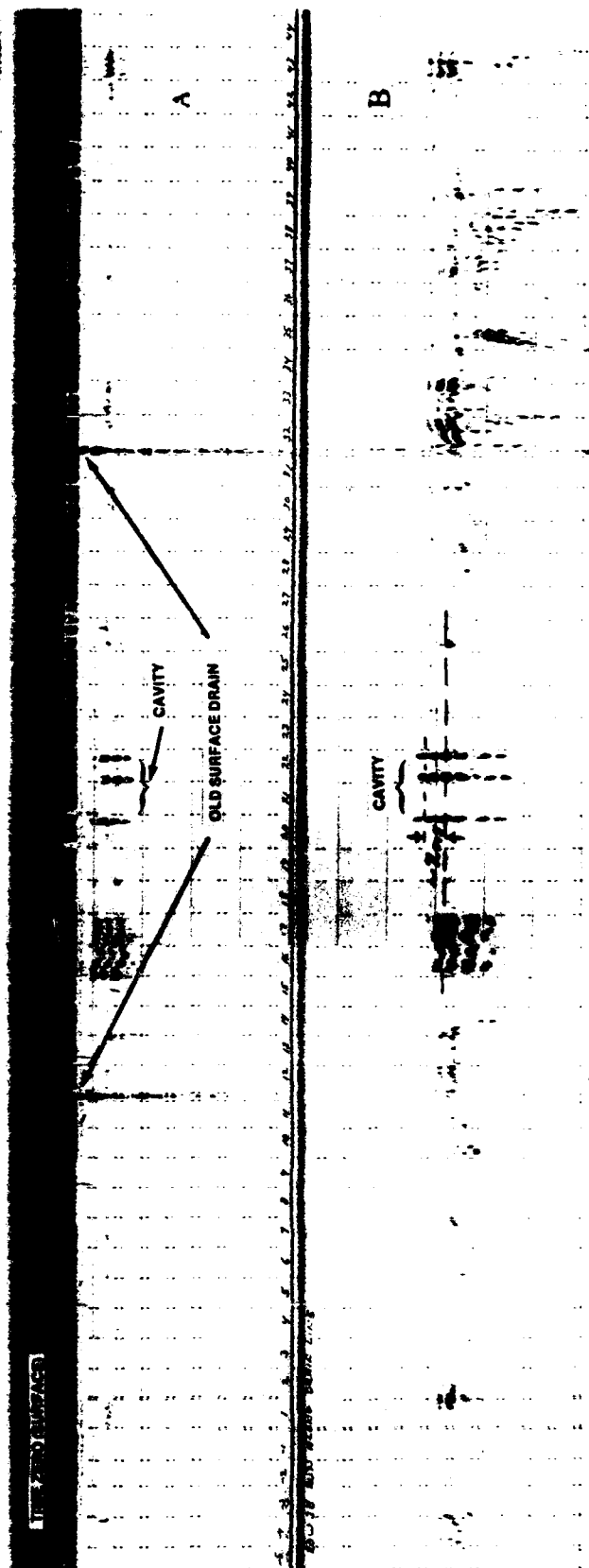


Figure 22. Portion of radar profile on row 3B from slab 5 to slab 44 over a 30-in. drain line. The scale lines are 5 ns apart.

key joint crossings, which are typically 20 ft apart. The closely spaced event marks between slabs 11 and 12 and slabs 31 and 32 show where the radar crossed the abandoned surface drain trench (Fig. 2). Note that the event marks do not always carry through both traces; this is simply a recorder malfunction. The letters a-f mark the fuel pits on this run. The fuel pit slabs produce a unique signature because there are steel utility lines rising to the surface and, as we discovered later, because some slabs are reinforced. This steel reflects and scatters the transmitted EM wavelet, blocking its downward flight. As a result, subsurface detail is partly or totally lost under these slabs.

At position D two slabs compose the fuel pit, while at the other stations the fuel pit consists of one slab. A similar arrangement can be seen in Figure 2 for row 15A. The concrete bottom is shown in both trace A and B. In trace B the horizontal dotted line represents the concrete bottom. This horizon is the reference plane which will be used to determine if a cavity exists under the pavement. As previously discussed, this horizon will move upward over a cavity, and because the amplitude of the reflected EM wavelet will become larger at a concrete/air boundary, the graphic display will also be darker.

A buried fuel pipe parallel to the path of the survey is also shown in the record. The long-period undulation in the pipe return occurred partly because the antennas did not ride directly over the top of the pipe, but moved at a varying distance to one side of the pipe. As a result the slant range or the EM wave travel time from the antennas to the pipe varied along the survey route.

The high-frequency variation, or short-period undulation, in the pipe return under slabs 29-40 is the result of changing subsurface conditions that affect  $V$  and  $\epsilon'$ . The same effect is shown in Figure 20. Here the antennas were towed over the drain line under row 18K. The system gain was set too low for a good pipe reflection to appear in the upper trace. Nevertheless, the pipe reflection in this trace is visible, especially on the right. Note that at each key joint the pipe appears to bend downward. This effect is caused by an increase in the real effective dielectric constant of the subgrade under the joints, which in turn decreases the propagation velocity of the EM wavelet. The burial depth of the pipe has not changed, but the travel time of the EM wavelet to and from the pipe has increased. The variation in EM wavelet velocity, or flight time, was caused by a variation in the moisture content of the subgrade. At the joints, rainwater freely entered and drained downward into the subgrade. This raised the moisture content of the sand, which in turn increased  $\epsilon'$

and (from eq 2) decreased  $V$ . The effect was that the travel time of the EM wavelet to and from the buried pipe was about 2.4 ns more under the joints than under the center of the slabs, where the sands were dryer.

Examples of radar profiles in which cavities were detected are shown in Figures 21-27. The radar profile along the 30-in. drain line under row OM (the southernmost drain line on the apron) is shown in Figure 21. As shown, a cavity was detected under slabs 9 and 10. Note that the concrete bottom appears to have moved upward about 2 ns and that the graphic record is darker at the position of the cavity, for reasons previously discussed.

A radar profile along the 30-in. drain line on row 3B is shown in Figure 22. On this run, three cavities were detected, one under slab 20 and two under slab 22. The strong return seen in trace A at the location of the old surface drains is due to the metal catch-basin grates. These grates reflect the EM energy back to the antenna and cause the "ringing" depicted by the dark banding.

The radar profile along the drain line under row 5G is shown in Figure 23. Over this line, 13 cavities were detected, 11 of which are shown. An enlargement of the graphic record next to cavity 11 under slab row 21 is shown in Figure 25. From the 2-ft event marks in trace A it is estimated that the cavity was about 8 ft wide.

Figure 24 shows the radar profile along row 7J. Four cavities were detected under the pavement on this run. A radar profile run to determine the width of the cavity under slab 6 is shown in Figure 26. From the 2-ft event marks in trace A, the width of the cavity at the profile crossing was determined to be about 6 ft.

The radar profile along fuel pit row 17A is shown in Figure 27. A cavity was detected under slab 7, the site of which is shown in Figure 28. The odd shape of this cavity, determined from the radar mapping procedure previously discussed, is shown in Figure 29. To verify this shape, two 6-in.-diameter holes were cored through the slab, one at the outer edge and one near the center. The core hole at the outer edge broke through the pavement exactly on the lip of the cavity. Into this hole was lowered an electric light, and a viewing mirror was lowered through the center hole. Visual inspection of the cavity was thus possible, and this verified that the shape of the cavity was as mapped out on the surface. The slab thickness was measured to be 14 in., and the cavity was found to be 9 in. deep. The unique feature of this cavity was that it had quite steep sides and the floor was a flat concrete surface on which there were a few small pebbles and a dusting of sand. The concrete floor is the top of a fuel-line utility box that connects to fuel pit A on slab 6.

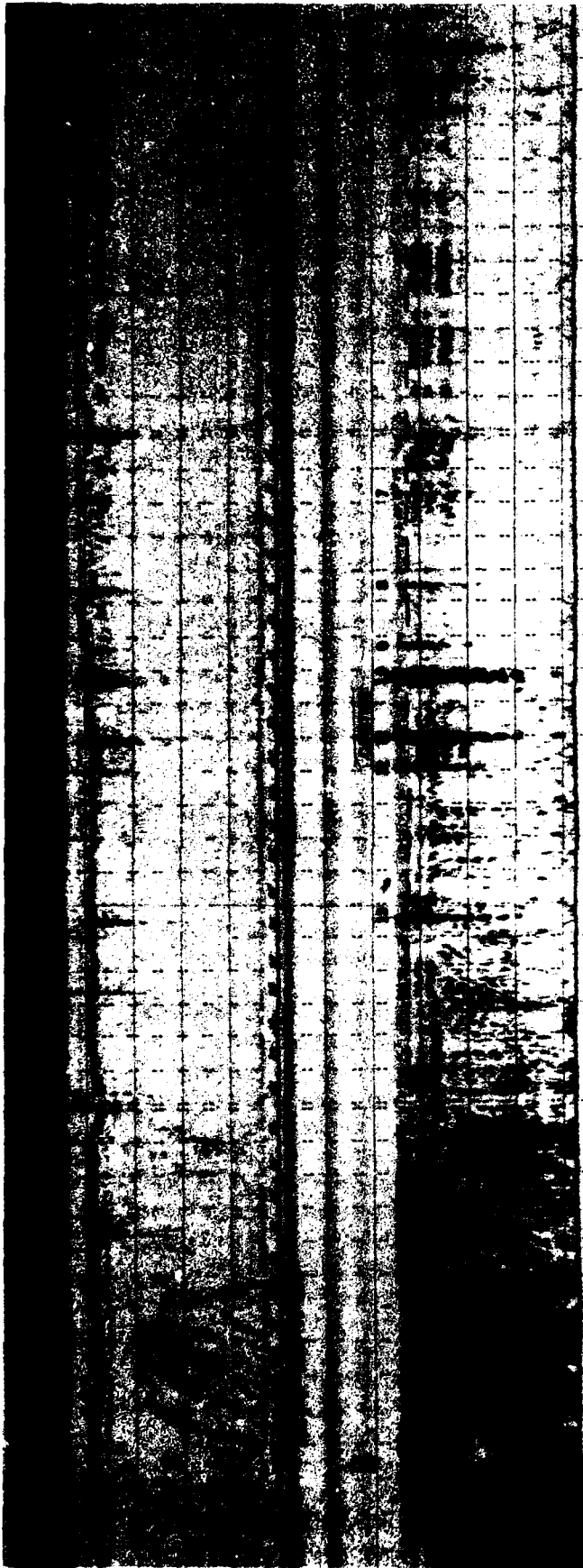


Figure 23. Portion of radar profile on row 5G between slab 44 and slab -1 over a 30-in. drain line. The scale lines are 5 ns apart.

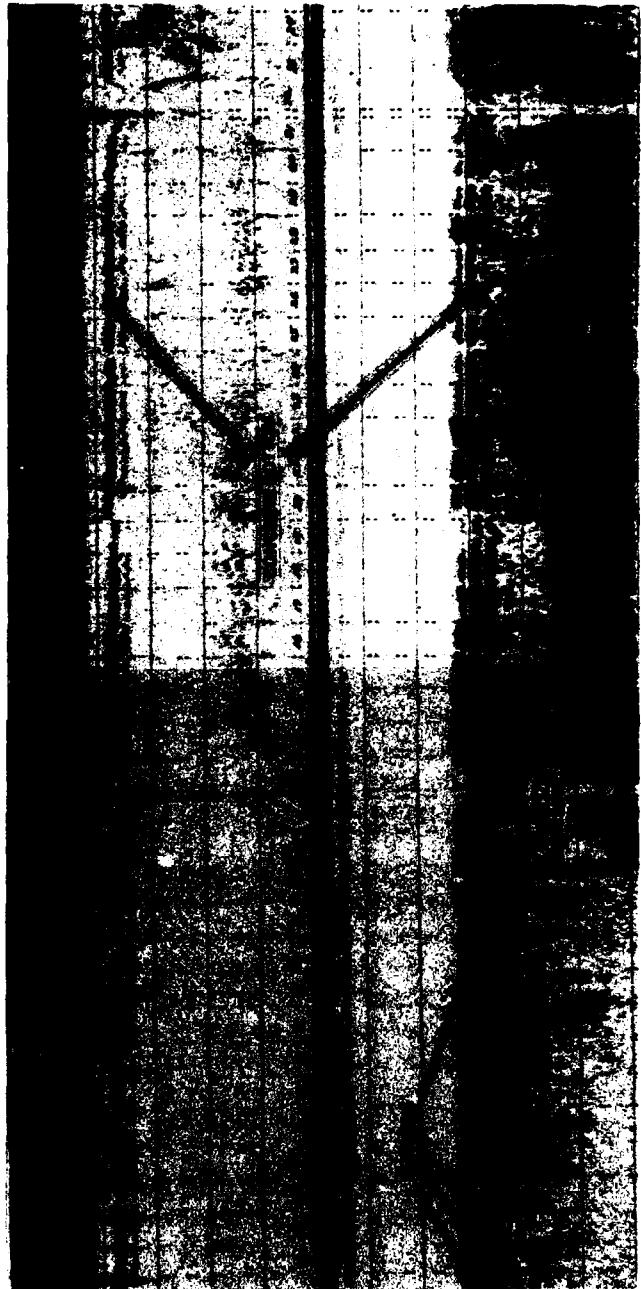
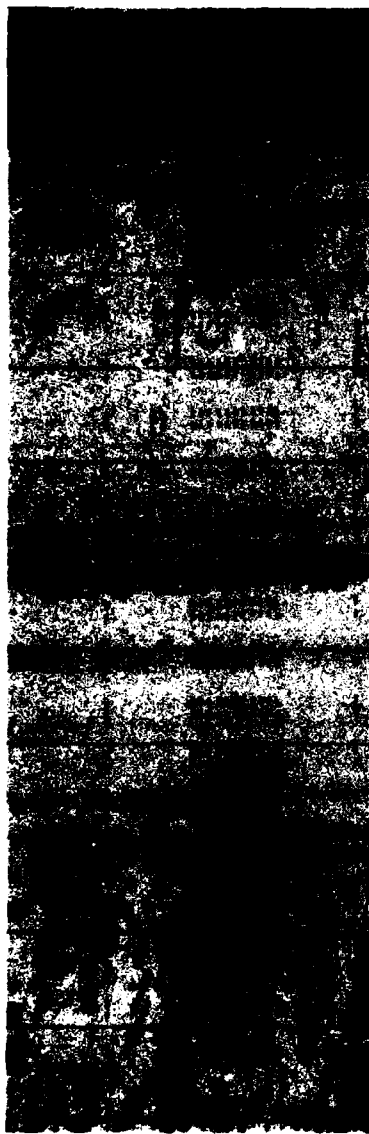
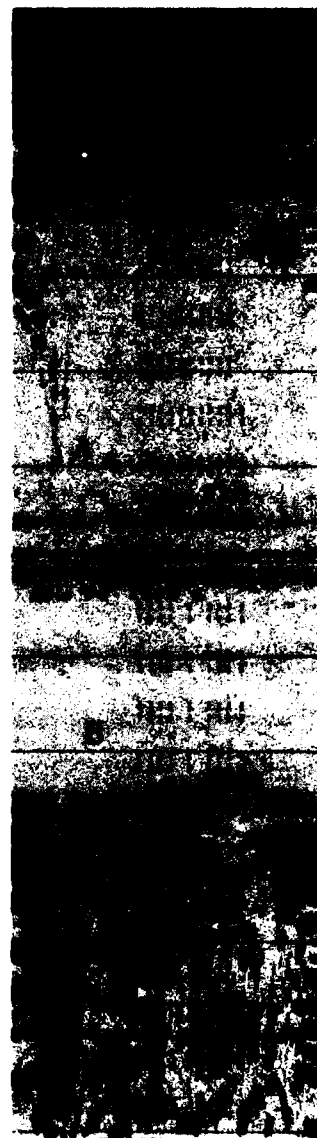


Figure 24. Portion of radar profile on row 7I between slab -3 and slab 34 over a 30-in. drain line. The scale lines are 5 ns apart.



*Figure 25. Radar scan across cavity under slab 21 of row 5G. The profile was run on slab row 21 on slabs 5E-H. The scale lines are 5 ns apart.*



*Figure 26. Radar scan across cavity under slab 6 of row 7J. The scale lines are 5 ns apart.*

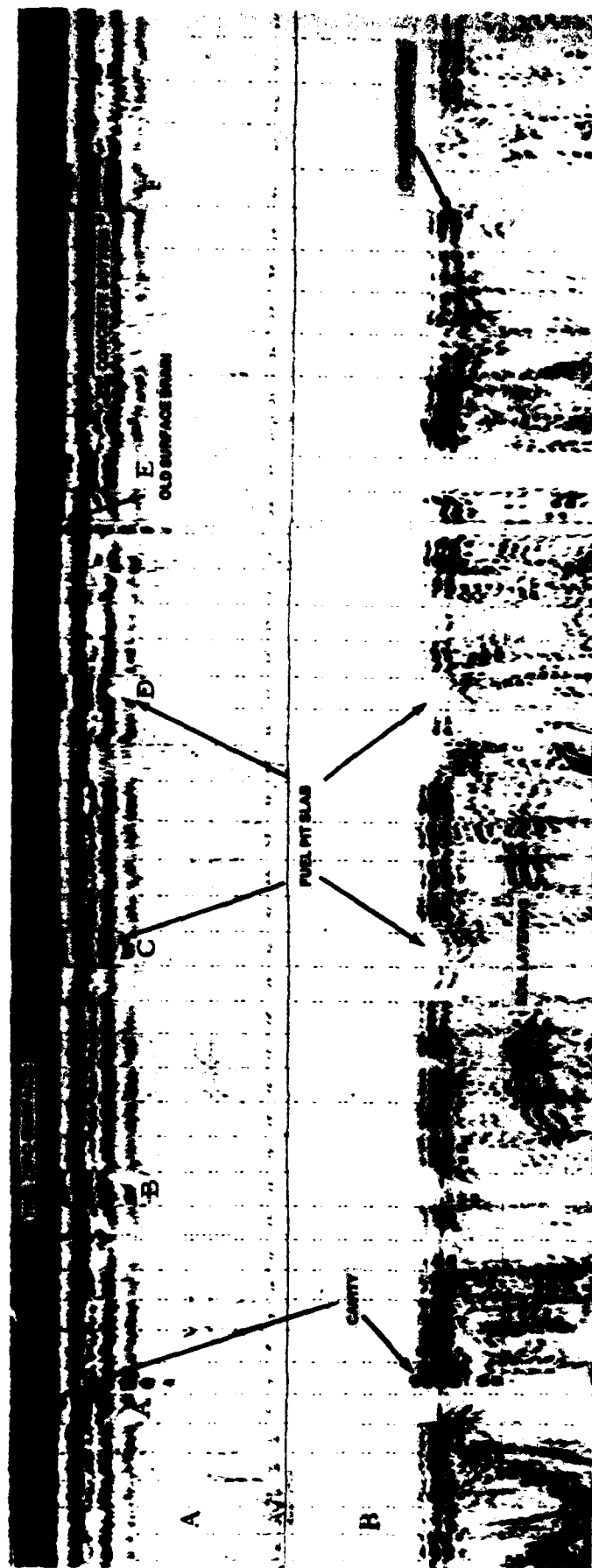


Figure 27. Radar profile on row 17A between slab 1 and slab 44. The scale lines are 10 ns apart.

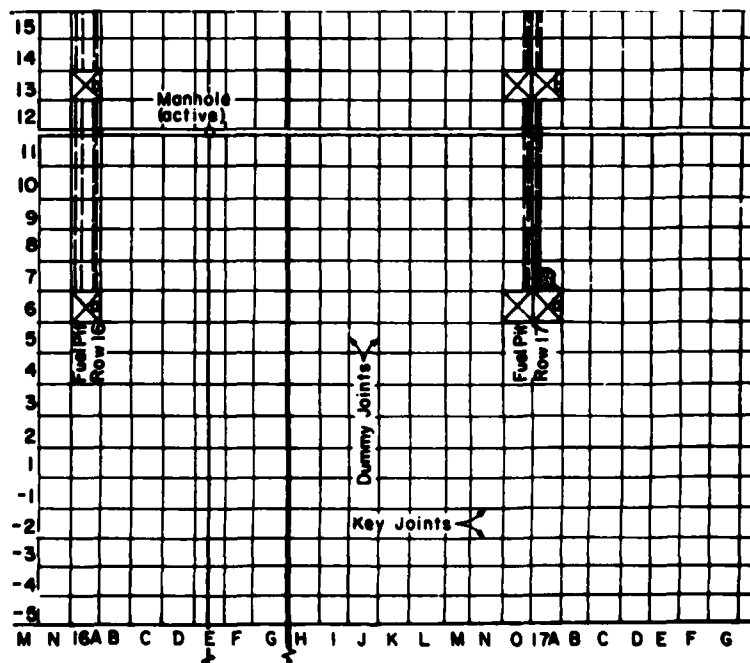
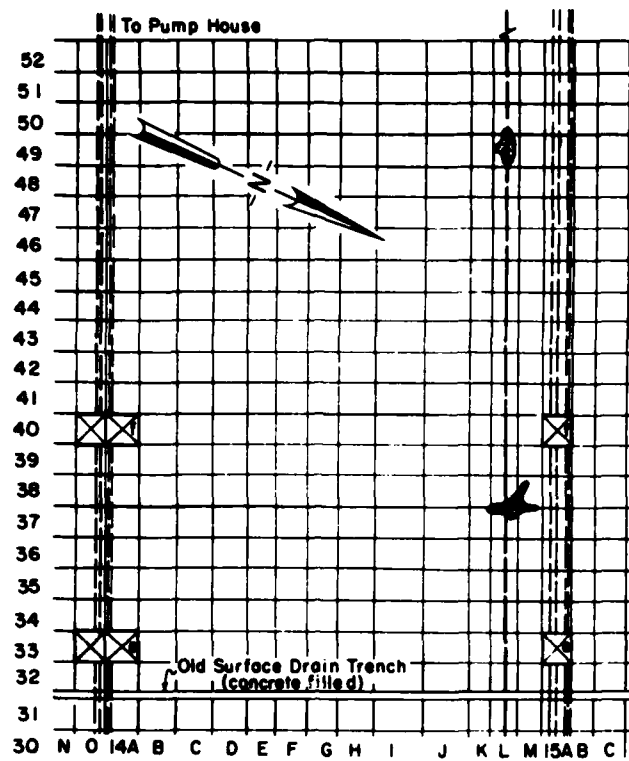


Figure 28. Location of cavities (hatched areas) under rows 14L and 14M and 17A.



*Figure 29. Configuration of cavity under slab 7 of row 17A determined by radar profiling.*

The radar profiling revealed 28 cavities, not including the cavity found by the base maintenance personnel. The location and dimensions of all the cavities are given in Table 1. The largest cavity was the original one found under slabs 37 and 38 on rows 14L and M during routine pavement repairs (Fig. 28). This cavity was somewhat cross-shaped, with arms over 20 ft long, and was situated over an abandoned water main (Fig. 28). Farther west along this pipe another cavity was found under slabs 49 and 50 on row 14L (Fig. 28). This was the second largest cavity, having dimensions of about 8 by 15 ft by 15 in. The deepest cavity measured was 23 in. under slab 19 of row 5G. Some cavities may, however, have been deeper than shown in Table 1, since only one drill hole measurement was generally made.

The relative locations of the cavities are shown in Figure 30. It is apparent in this figure that all but one cavity developed in association with a buried utility. All but two cavities were located over water pipes. Of these two cavities, one was located over a utility box under slab 6 on row 17A. The only cavity not associated with a buried utility was located on the apron taxiway under slab 51 on row 8J just east of taxiway 3.

All cavities except the one under slab 1 on row 9J and the two located under the runway pavement were grout-filled in November 1982. About 35 yd<sup>3</sup> of grout was used. The remaining three cavities are also to be grout-filled. In addition the 30-in. drain

lines are to be inspected and repaired where subgrade material is found to be entering or where there are breaks in the lines. Mr. Smart of base maintenance told us that internal banding and grouting of the pipe joints under the north end of the runway had been required several years earlier. The pipe was found to be filled with sand that had been washed into the pipe through the open joints. Presumably the same problem exists where cavities were detected over all other drain lines and the utility structure on row 17A. The cause of the small cavity on the apron taxiway may be poor compaction of the subgrade sands. Rearrangement and consolidation of this material may have occurred due to heavy aircraft traffic coupled with water migration through the pavement joints. Another maintenance program planned for 1983 is a rehabilitation of the parking apron pavement expansion joints from fuel pit row 12 through 21. Further work is planned for 1984. All old joint and crack sealant will be replaced. This should stop surface drainage under the slabs and further movement and rearrangement of the subgrade material.

Only once did the graphic record indicate a cavity where one did not exist. This feature appeared as the radar was pulled across fuel pit slab 33 on row 4A. The concrete bottom rose upward about 2.5 ns under the slab (Fig. 31). Coring through the concrete (Fig. 32) revealed that the slab was reinforced with a 5/8-in. steel bar (Fig. 33). This was surprising because the as-built drawings show that no reinforcing bar was

Table 1. Location and sizes of subpavement voids.

Row	Slab	Concrete thickness (in.)	Void depth (in.)	Approximate cavity size (ft)
0M	9/10	12	8	3.5X15
1A	12	13	1.5	2X2
3B	20	13	4	2X2
3B	22 (east side)	13	7	-
3B	22 (west side)	13	7	-
5G	-4	-	3.5	2X2
5G	-3	-	6	2X2
5G	-2	-	4	2X2
5G	-1	12	11	10X10
5G	1	-	2	4X4
5G	2	-	1	4X4
5G	13/14	-	8	4X4
5G	16	-	6	2X2
5G	18	14	6	4X4
5G	19	-	23	10X10
5G	21	14	5	8X8
5G	22	14	8	4X4
5G	26	-	6	5X5
7J	-4/-3	14	8	3X11
7J	-3/-2	14	4	4X4
7J	-2/-1	14	6	6X6
7J	6	14	9	10X10
8J	51	-	2	2X2
9J	1	not drilled		3X3
14L&M	37/38*	14	8	20X20
14L	49/50*	13	15	8X15
17A	7*	14	9	8X11

On runway over north drain line,  $\approx$  2-ft-diameter cavity on west side of first slab east of center line and  $\approx$  2-ft-diameter cavity on west side of first slab west of center line (Fig. 30).

\*See location in Figure 28.

used. This finding points up the fact that anomalous subsurface conditions can exist which may be misleading during a cavity detection survey. It also demonstrates why drill hole verification of one's interpretation of the radar record is highly desirable. This is true for the dual-antenna radar profiling arrangement used in this study but is most important when a single transceiver antenna is used. When the latter is used, many "bright spots" or anomalous features appear which may be interpreted as cavities when in fact none exist. Some factors that complicate interpretation of the radar data from a transceiver antenna are impulse time length, void thickness, multiple reflection overlap and changing subsurface conditions (Clemens and McGhee 1980, More et al. 1980, Alongi et al. 1982). These complications are reduced or eliminated with the dual-antenna refraction method used in this study.

Features in the transceiver antenna graphic record that could be misinterpreted as a cavity are seen

in Figure 23 between slabs 35 and 36 and in Figure 24 between slabs 34 and 35. Note how these "bright spots" stand out and have characteristics similar to the real cavity features. However, neither of these features produced the time hump in the receive-only antenna record indicative of a cavity. We attribute these bright spots in trace A to increased subgrade wetness under the key joints.

Figure 34 shows other examples of features that appeared in the single-transceiver antenna graphic record that can be or have been misinterpreted as cavities. In each case the anomalous feature in trace A does not produce the hump in the receive-only antenna graphic record that signifies a cavity. Drill hole measurement and inspection was used to verify that these features were not cavities.

The signatures of slab joints are highlighted in Figure 34a and b. The arrows in Figure 34b point to metal targets in the concrete. The center one was a buried reinforcing bar; the outer two were steel



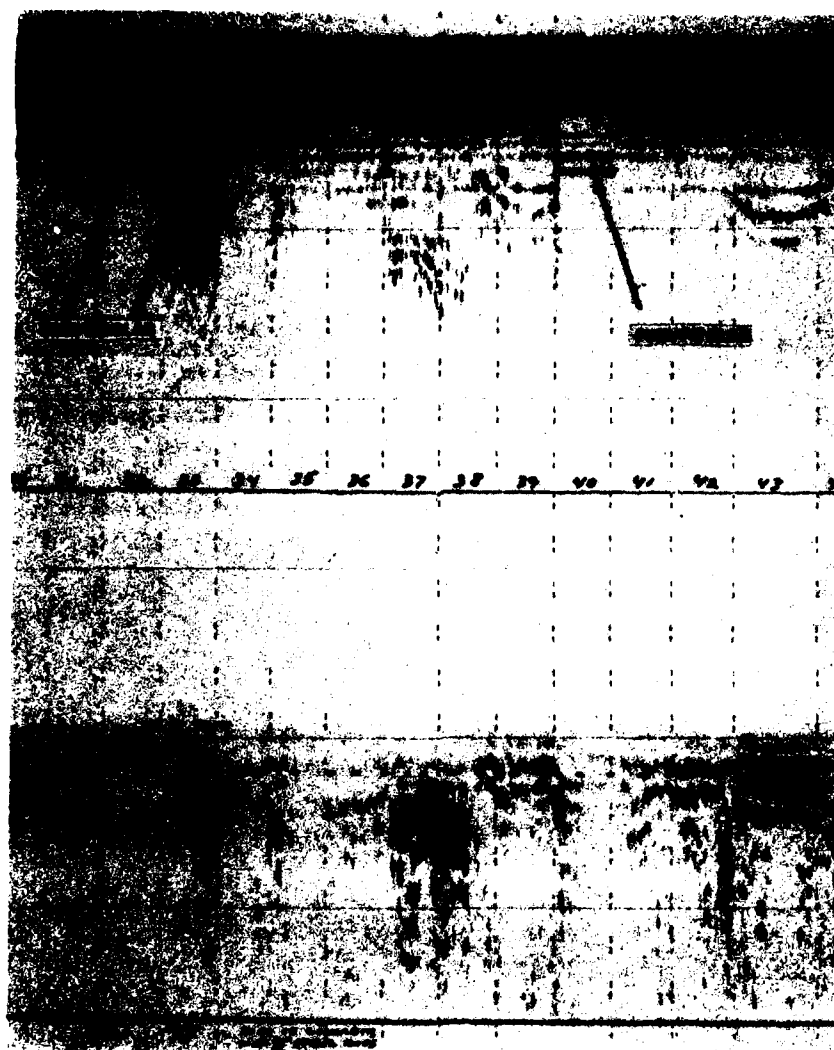


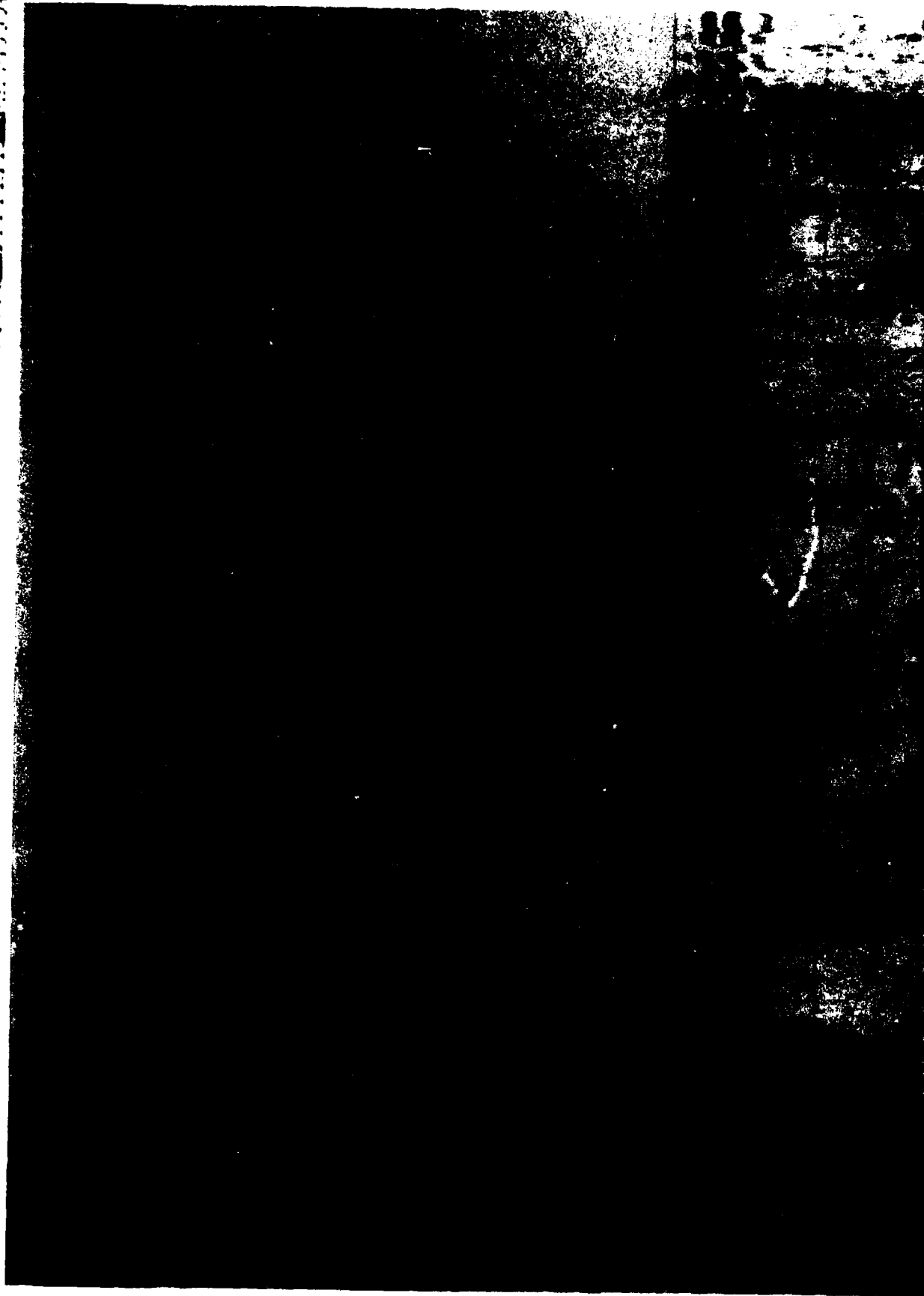
*Figure 31. Portion of radar profile on row 4A between slabs 30 and 44. The scale lines are 10 ns apart.*



*Figure 32. Layout of utility fixtures on slab 33 of row 4A and the pavement core taken to allow inspection of the concrete and the subgrade material.*

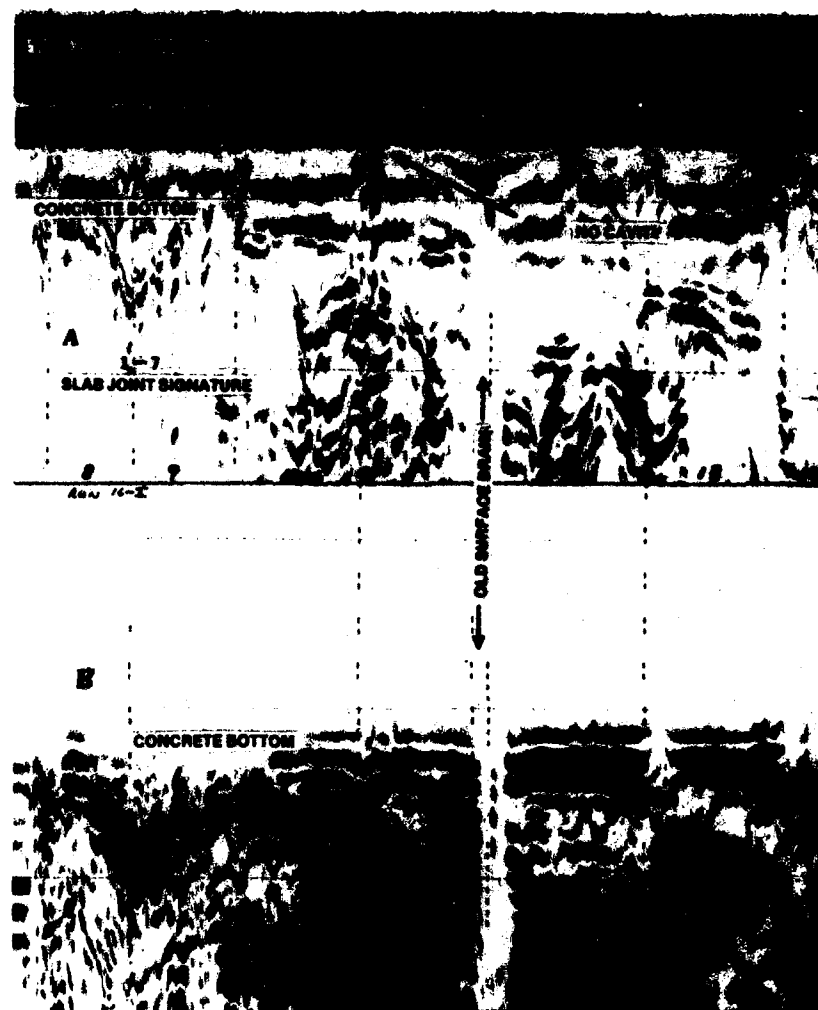


*Figure 33. Row 4A, slab 33 pavement core. The arrow points to a 5/8-in.-diameter steel reinforcing bar.*



a. Joint signatures.

Figure 34. Radar profile records showing slab joint features, metal targets and other subsurface reflection signatures that can be misinterpreted as cavities under concrete pavement.



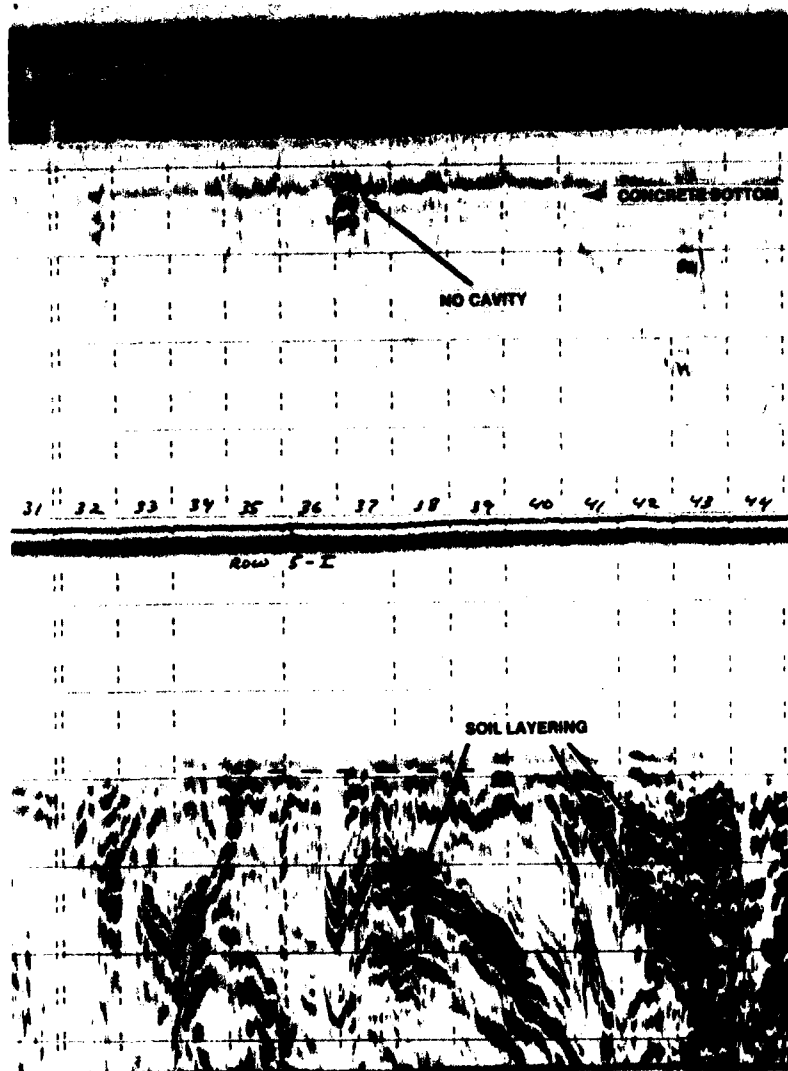
*b. Joint signatures and steel objects.*

*Figure 34 (cont'd). Radar profile records showing slab joint features, metal targets and other subsurface reflection signatures that can be misinterpreted as cavities under concrete pavement.*



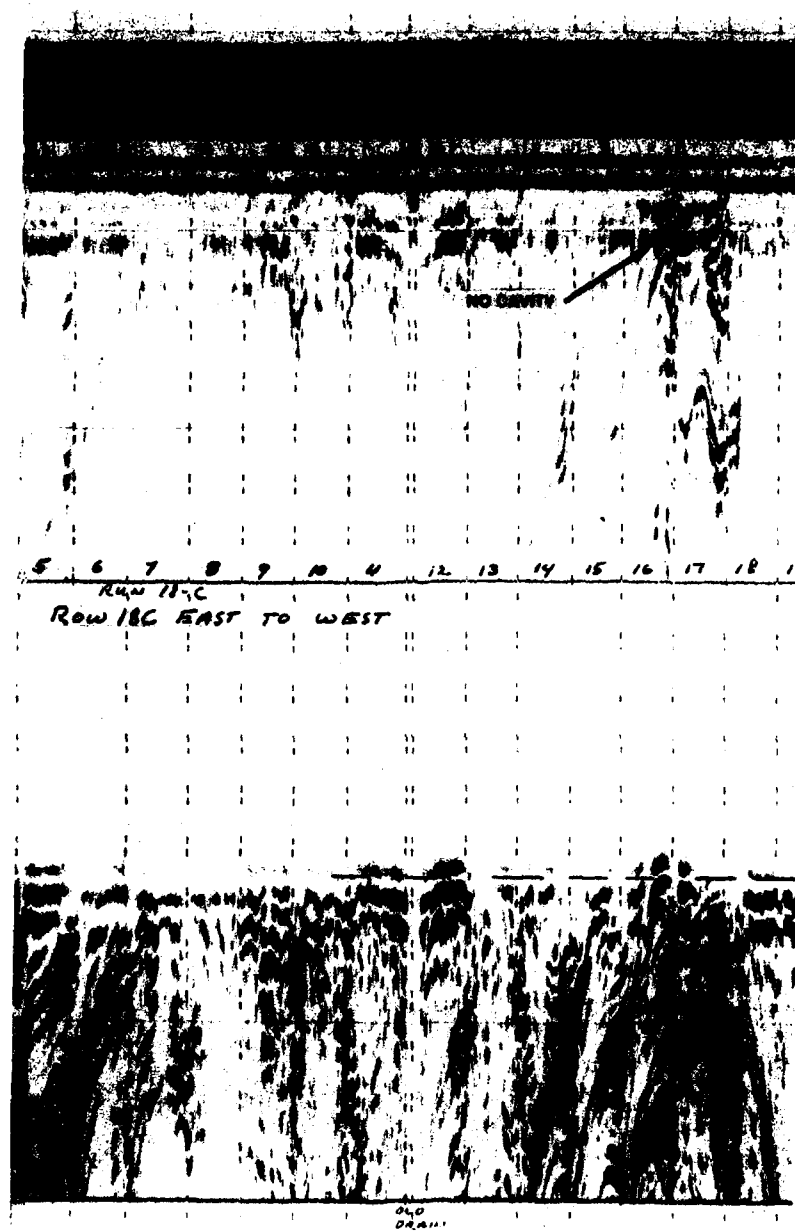
c. Soil layering along row 9K.

Figure 34 (cont'd).



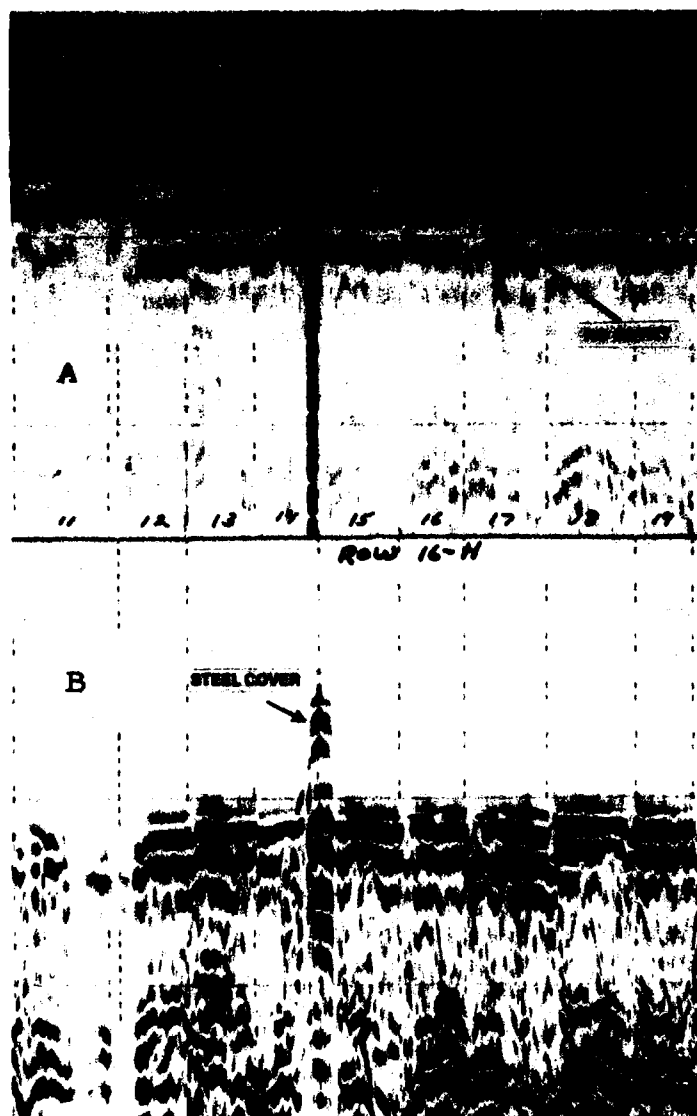
d. Soil layering along row 51.

Figure 34 (cont'd). Radar profile records showing slab joint features, metal targets and other subsurface reflection signatures that can be misinterpreted as cavities under concrete pavement.



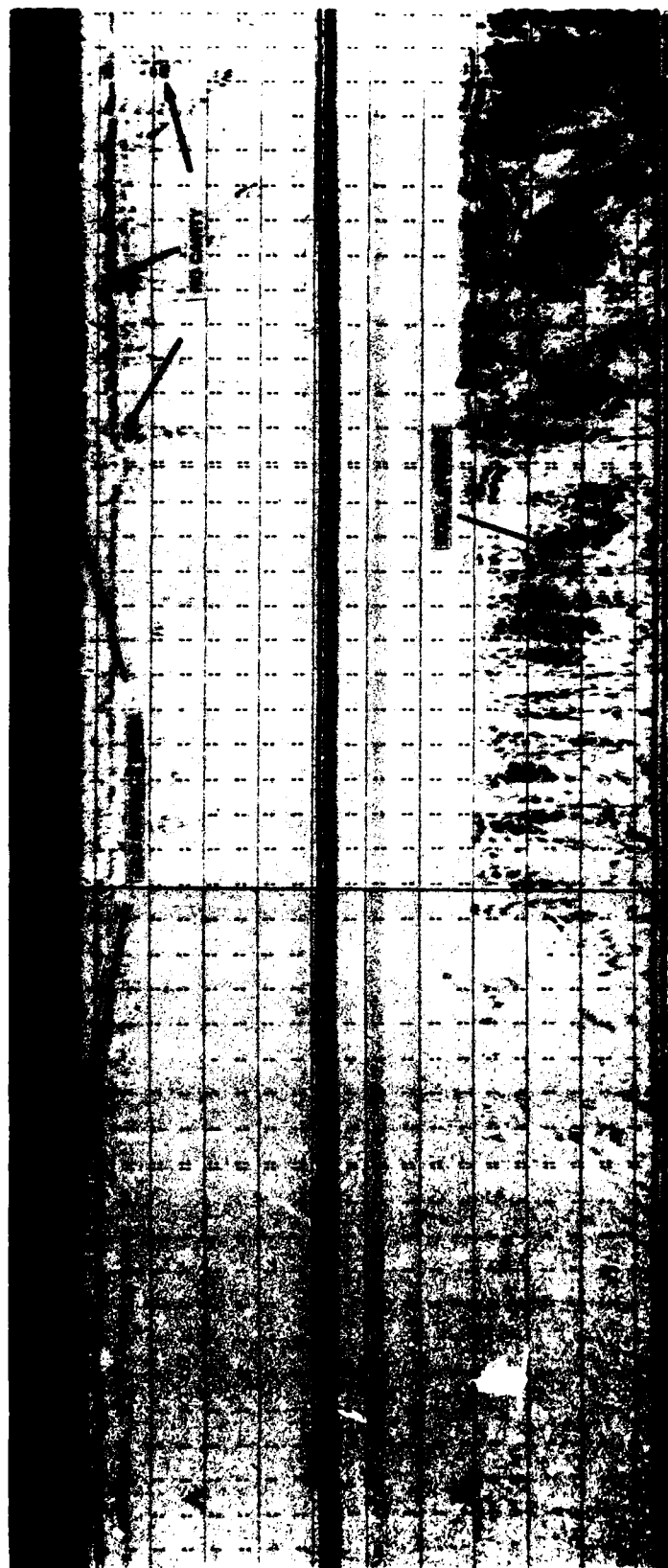
e. Old drain.

Figure 34 (cont'd).



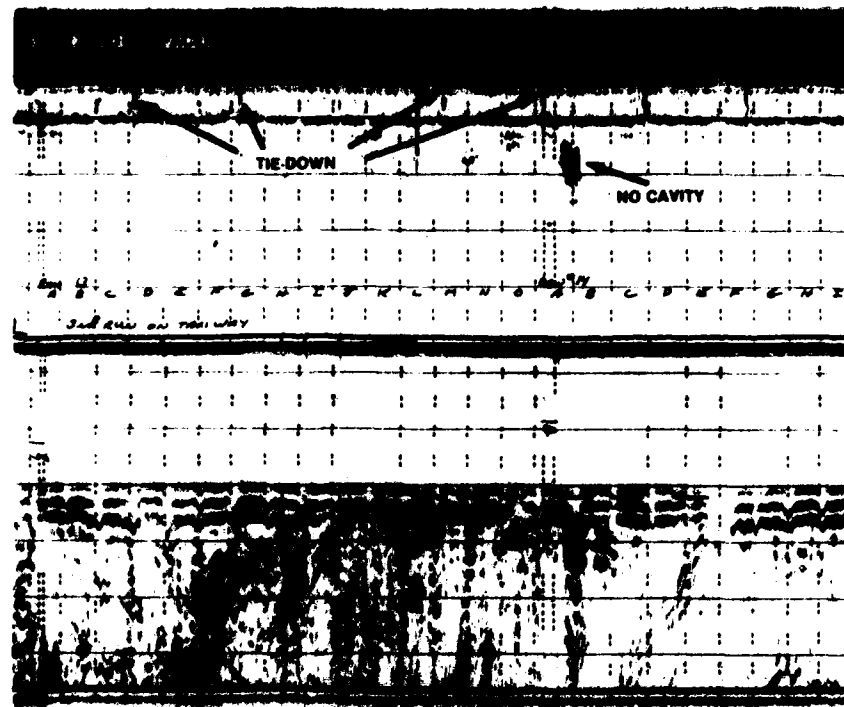
*f. Steel cover.*

*Figure 34 (cont'd). Radar profile records showing slab joint features, metal targets and other subsurface reflection signatures that can be misinterpreted as cavities under concrete pavement.*



*g. Old surface drain and soil layering.*

*Figure 34 (cont'd).*



*h. Tie-downs.*

*Figure 34 (cont'd). Radar profile records showing slab joint features, metal targets and other subsurface reflection signatures that can be misinterpreted as cavities under concrete pavement.*

aircraft tiedowns. Other features shown are soil layers and the antenna ringing produced as an antenna was pulled across a steel cover.

On the apron taxiway many slabs were replaced with steel-reinforced concrete. The effect of this reinforcement is shown in Figure 35. Because the reinforcement is a good reflector or can scatter the transmitted EM energy, little energy "seeps" through the steel "screen," and even less arrives back at the antennas after being reflected from an interface below the reinforcement. This loss results in areas with no reflection data and white bands in the transmit impulse. These bands are caused by an antenna-loading effect produced by the close proximity of the steel reinforcement.

During our study several pavement sites which had settled were extensively profiled in an effort to detect subslab cavities. Figure 36 shows one of these sites, where two slab corners had subsided over an inch. In no case was a cavity detected in the radar graphic record, implying that the slabs had settled with or had already dropped onto the surface of the underlying sands. The lack of cavities was further verified by drill holes. Slab displacement at these sites was probably due to dynamic loading of the pavement by aircraft traffic, coupled with surface water drainage through open pavement joints; this reduced the shear strength of the sand, allowing consolidation of the subgrade.

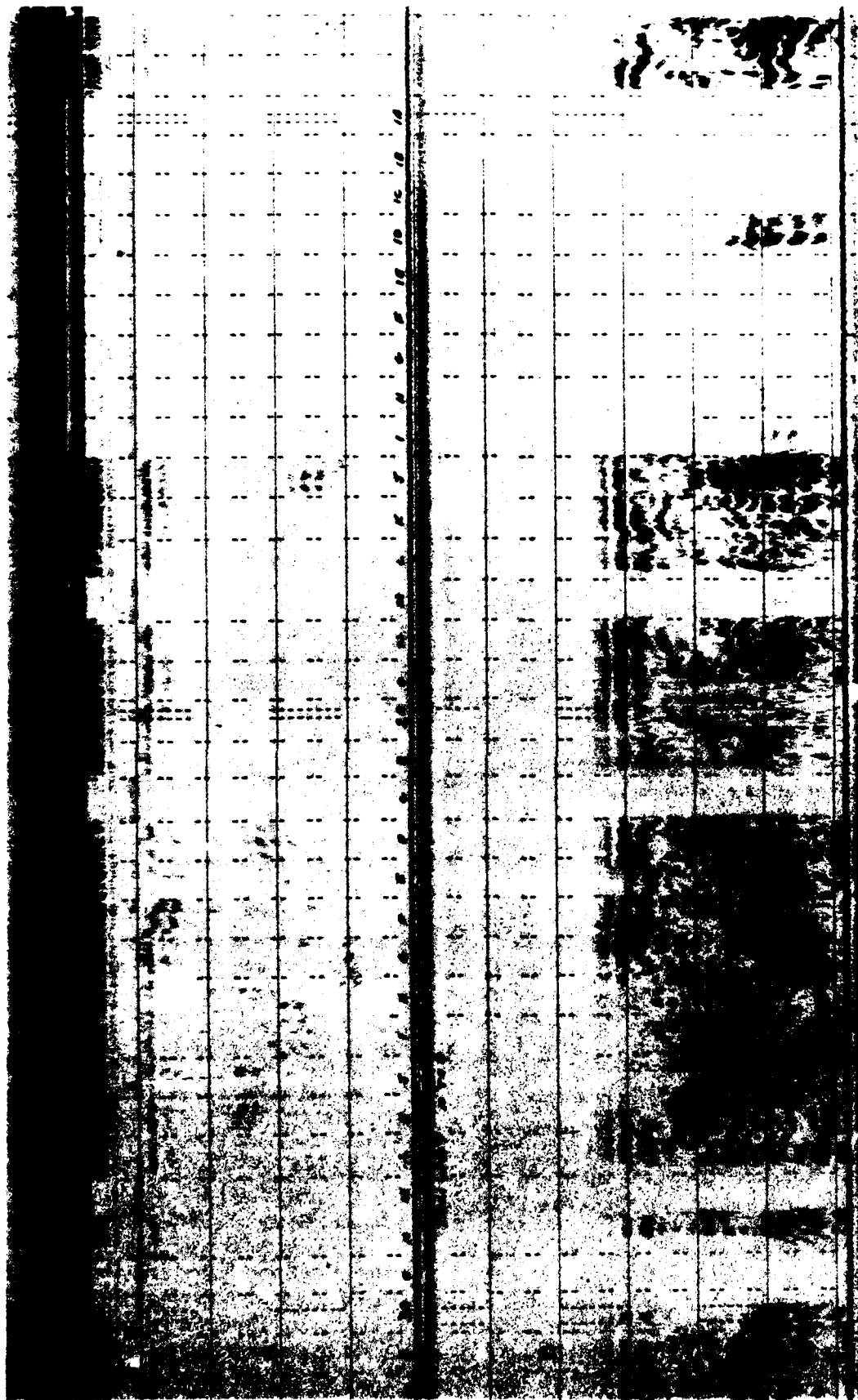


Figure 35. Radar profile record on apron taxiway. The scale lines are 5 ns apart.



*Figure 36. Corner slab failure. Arrows point to the sites where inspection holes were drilled.*

#### FALLING-WEIGHT DEFLECTOMETER TESTS

A falling-weight deflectometer (FWD) test was also made on five of the apron slabs. The device drops a weight, which strikes a spring system connected to a circular base plate that is resting on the pavement, producing a force impulse. Different drop heights and weights can be used to vary the maximum impact force, which is measured by an accelerometer on the base plate. The so-called pavement deflection bowl produced by the impact force is determined electronically by a series of velocity transducers spaced at intervals outward from the base plate (Fig. 37). The accelerometer and transducer data are analyzed by an onboard computer to provide on-site information on impact force and pavement deflection at each transducer position. These deflection data were later analyzed using statistical regression methods to construct the shape of the pavement deflection bowl.

In general, FWD test results are used in structural analyses to evaluate the bearing capacity and expected lifetime of a pavement system vs traffic usage and related wheel loadings (Koole 1979). Our use of the FWD was to determine if this nondestructive test could verify the presence of a subslab cavity detected in the impulse radar profile. In short the FWD test was used to determine the deflection responses of a slab with an underlying cavity and of slabs which were fully supported by the subgrade sand. Only one test series was made because the

FWD was not available to us for use at Plattsburgh AFB until all cavities on the parking apron had been grout-filled except under slab 1 of row 9J.

FWD tests were made on slab 1 of rows 9H, I, K and L as well as row 9J. The impact force was about 23,000 lbs or 210 psi under the 11.8-in.-diameter base plate. Six drop tests were made at the center of each slab. The deflection data for each slab were then averaged. The averaged deflection data from the FWD tests on supported slabs 9H, I, K and L and partially unsupported slab 9J are plotted in Figure 38a and 38b, respectively. The third-degree polynomial regression curves passing through the data in Figures 38a and 38b have correlation coefficients of 0.998 and 0.999, respectively. In Figure 38c the deflection curves are presented together. These curves show, as expected, that the partially unsupported slab deflected substantially more under the force impulse than the supported slabs. These results indicate that the FWD test may be used instead of drill holes to verify the existence of a subpavement cavity detected by impulse radar profiling. The FWD test may also be used as a substitute cavity detection device. It would, however, be much more time consuming to use than the radar system. The FWD tests at Plattsburgh AFB were limited in number. Further tests need to be made before the FWD can be considered to be an acceptable method for detecting or verifying the existence of cavities below concrete pavement slabs determined with impulse radar sounding.



*Figure 37. CRREL trailer-mounted falling-weight deflectometer. The drop weights, layered on the mast at the rear of trailer, are raised prior to release. Below the trailer are velocity transducers shown in contact with pavement. A portion of the circular impact plate is visible in contact with pavement under the center of the trailer axle.*

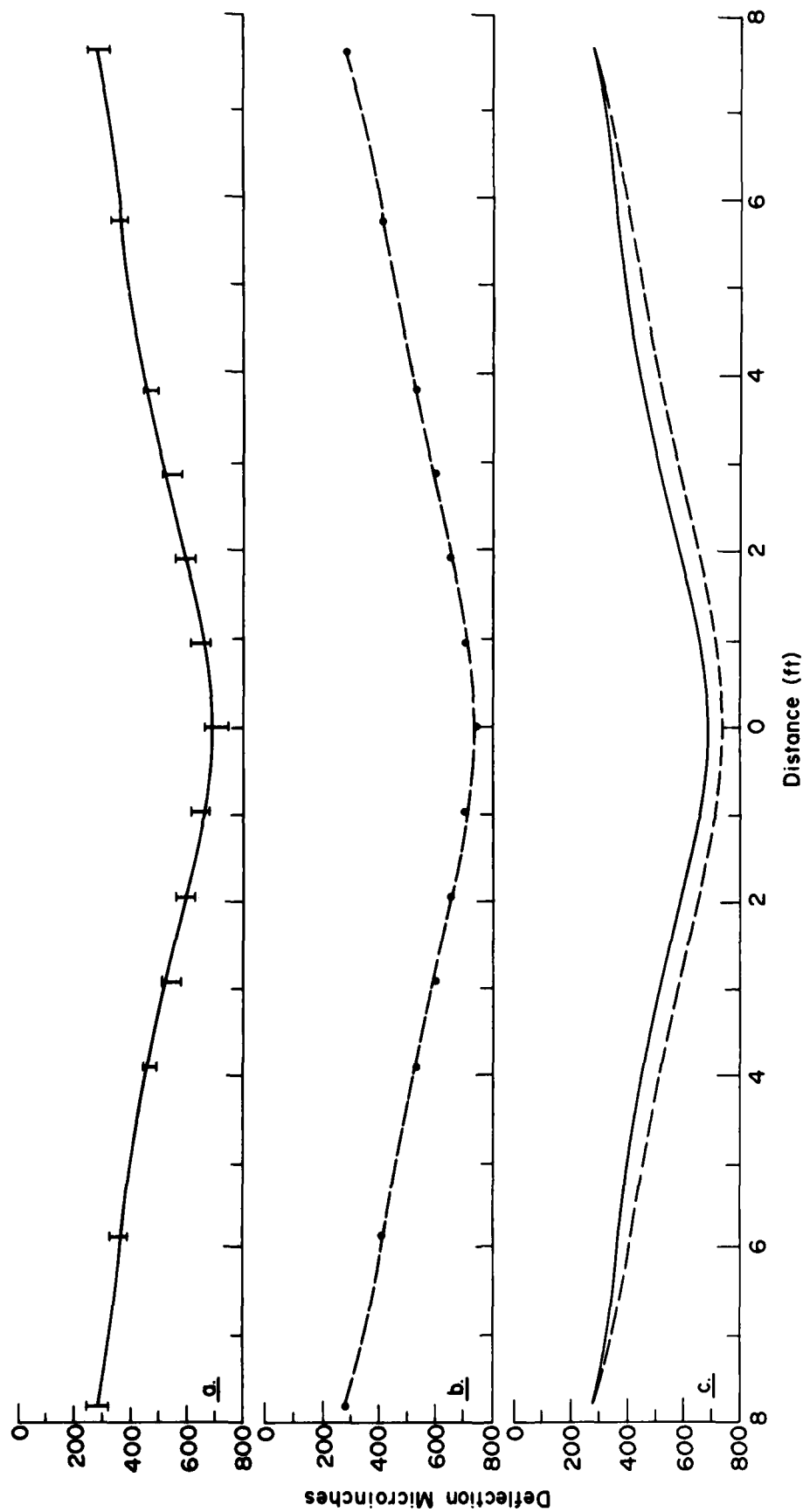


Figure 38. Deflection of four supported slabs (a) and one partially unsupported slab (b) vs distance from the center of the FWD impact plate. The bars in curve a represent the spread of the averaged FWD test deflection data from the four slabs.

## DISCUSSION AND CONCLUSIONS

An impulse-radar profiling system was evaluated for detecting cavities under the pavement at Plattsburgh Air Force Base, Plattsburgh, New York. The dual-antenna arrangement used was described and theoretical considerations presented to show that this antenna arrangement is ideally suited for detecting cavities under nonreinforced concrete slabs. The field study provided evidence that the unique dual-antenna system functioned as predicted; it detected 28 cavities below the pavement. Their existence was confirmed by direct drill-hole measurement and observation.

Impulse radar graphic records were presented which showed typical cavity features. Other profile records were presented to demonstrate that the use of a single-transceiver antenna for detecting sub-pavement cavities can result in interpretation difficulties and uncertainty. It is therefore recommended that a single-transceiver antenna not be used for detecting cavities under concrete pavement.

In addition, neither single- or dual-antenna arrangements appear suitable for detecting cavities or other interfaces below concrete reinforced with wire mesh or closely spaced steel reinforcing bars. This was shown to be the case in this study and in our cavity detection study on the Fort Wainwright Airfield, Fairbanks, Alaska (Kovacs and Morey 1982). However, further field trials with various antenna spacings and system gain settings and the use of antennas operating at a different frequency may provide a means of detecting cavities and other features under reinforced concrete pavement.

Follow-up IR scanning work by A.R. Greateorex as part of this study to detect voids under the parking apron did not produce positive results. Surface features such as old paint, repair patches, grout washings, concrete cutting residue, oil and fuel stains and concrete texture differences all produced contrasts in the IR image. These features complicated image interpretation and created so many surface contrasts that void detection was extremely difficult at best. IR scanning for voids at a location with thinner pavement may provide positive results.

Lastly, the summary results of the falling-weight deflectometer field test indicate, as expected, that a partially supported concrete slab undergoes more

deflection under an impulse force than a fully supported slab does. The results suggest that an FWD test may be used as a nondestructive method to verify impulse radar results showing a cavity under concrete pavement slabs.

## LITERATURE CITED

- Alongi, A.V., T.R. Cantor, C.P. Kneeter and A. Alongi, Jr. (1982) Concrete evaluation by radar theoretical analysis. *Transportation Research Record* 853.
- Clemens, G.G. and K.H. McGhee (1980) Applicability of radar subsurface profiling in estimating sidewalk undermining. *Transportation Research Record* 752.
- Dean, A.M., Jr. (1982) Inspection of a void beneath apron slabs at Plattsburgh AFB: Impulse radar survey demonstration. CRREL Internal Report.
- Greateorex, A.R. (1982) IR location of voids below the aircraft parking apron, Plattsburgh AFB. CRREL Internal Report
- Koole, R.C. (1979) Overlay design with the falling weight deflectometer. Presented at Annual Meeting of the Transportation Research Board, Washington, D.C.
- Kovacs, A., A.J. Gow, J.H. Cragin and R.M. Morey (1982) The brine zone in the McMurdo Ice Shelf, Antarctica. CRREL Report 82-39.
- Kovacs, A. and R.M. Morey (1982) 1980 radio echo sounding study. In *Fort Wainwright, Alaska North Runway Pavement Study* (D.A. Gaskin, Ed.). CRREL Contract Report prepared for U.S. Army Engineer District, Alaska.
- More, J.R., J.D. Echard and C.G. Neill (1980) Radar detection of voids under concrete highways. IEEE International Radar Conference, The Institute of Electrical and Electronic Engineers, New York, New York.
- Morey, R.M. (1974) Continuous subsurface profiling by impulse radar. American Society of Civil Engineering, Engineering Foundation Conference on Subsurface Exploration for Underground Excavation and Heavy Construction, Henniker, New Hampshire.
- Sellmann, P.V. (1982) Inspection of a void beneath apron slabs at Plattsburgh AFB. CRREL Internal Report.

A facsimile catalog card in Library of Congress MARC format is reproduced below.

Kovacs, Austin

Detection of cavities under concrete pavement / by Austin Kovacs and Rexford M. Morey. Hanover, N.H.: U.S. Cold Regions Research and Engineering Laboratory; Springfield, Va.: available from National Technical Information Service, 1983.

v, 49 p., illus.; 28 cm. ( CRREL Report 83-18. )

Prepared for Office of the Chief of Engineers by Corps of Engineers, U.S. Army Cold Regions Research and Engineering Laboratory.

Bibliography: p. 41.

1. Cavities. 2. Concrete. 3. Pavement. 4. Radar. I. Morey, Rexford M. II. United States. Army. Corps of Engineers. III. Cold Regions Research and Engineering Laboratory, Hanover, New Hampshire. IV: Series: CRREL Report 83-18.

**END**

**FILMED**

**9-83**

**DTIC**